AN ATTEMPT TO MEASURE THE ELECTRON TEMPERATURE OF A XENON CHLORIDE EXCIMER LASER DISCHARGE PLASMA BY THOMSON SCATTERING

by

MICHAEL KON YEW HUGHES

B.Sc. (Eng), Queen's University (Kingston), 1990

A THESIS SUBMITTED IN PARTIAL FULFILLMENT OF

THE REQUIREMENTS FOR THE DEGREE OF

MASTER OF APPLIED SCIENCE

in

THE FACULTY OF GRADUATE STUDIES

Department of Physics

We accept this thesis as conforming
to the required standard

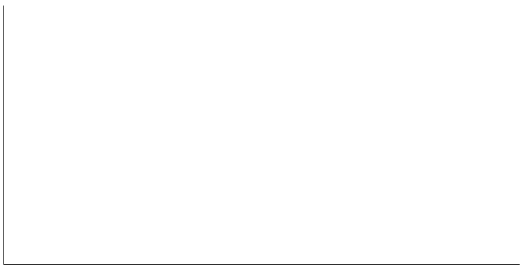

THE UNIVERSITY OF BRITISH COLUMBIA

July 1993

© Michael Kon Yew Hughes, 1993

In presenting this thesis in partial fulfilment of the requirements for an advanced degree at the University of British Columbia, I agree that the Library shall make it freely available for reference and study. I further agree that permission for extensive copying of this thesis for scholarly purposes may be granted by the head of my department or by his or her representatives. It is understood that copying or publication of this thesis for financial gain shall not be allowed without my written permission.

(Signature) _____

Department of Physics

The University of British Columbia
Vancouver, Canada

Date 18 August 1993

DE-6 (2/88)

Abstract

An electronic timing system was developed so that a commercial Nd:YAG regenerative amplifier could be triggered remotely with a BNC cable and pushbutton switch. This system was used to accurately time a Xenon Chloride transverse discharge laser to the short, high power Nd:YAG pulse to within 5 ns.

Attempts were made to determine the electron velocity distribution of the discharge plasma of this Xenon Chloride laser using the method of Thomson scattering. The Thomson scattering parameter α was 0.22. A short, 532 nm pulse was injected into the excimer laser and the backscattered light was analysed. The scattered beam was imaged onto the entrance slit of a spectrometer and the spectrally dispersed output was collected by either a streak camera or a photomultiplier array.

The injection laser pulses were produced by amplifying the 100 ps pulses from a modelocked Nd:YAG laser in a regenerative amplifier giving probe pulses of approximately 40 mJ in 100 ps at the excimer laser.

Aside from the signal intensity at shifted wavelengths which was measured to give an estimate of the electron temperature, the relative timing of the probe pulse to the excimer current was measured to give a time profile of the temperature. The injection pulse power and excimer laser current were also needed to ensure that results behaved as predicted in relation to these parameters.

The temperature measurements proved to be impossible due to extremely high noise levels, a lack of resolution of the spectrometer and possibly laser heating effects.

Table of Contents:

List of Figures:

List of Tables:

1 Introduction

This work follows the acquisition of a regenerative amplifier which made possible the production of short, high power, 1064 and 532 nm light pulses at rates up to 10 Hz. To use this new amplifier system, it was necessary to understand its internal timing and to determine the synchronization pulses available to external timing devices. This knowledge was used to accurately synchronize the regenerative amplifier, the discharge laser pulses, and the measurement devices.

In previous experiments, synchronization was left to chance. This was possible because probe pulses were produced at intervals of tens of nanoseconds making it possible to capture a pulse within the discharge laser pulse which was tens to hundreds of nanoseconds long. Such synchronization is not possible with a repetition rate of only 10 Hz. This thesis describes how such timing was achieved.

This work has applications in many experiments in which accurate synchronization is necessary. It is relevant to experiments investigating laser produced plasmas or work in which the pulses of two lasers must be synchronized such as in the Thomson scattering experiment to be described. A method for accurate timing is needed to fully utilize the high power short pulses now available.

Once the system was in place to limit the timing uncertainty to under 5 ns, attempts were made to use the method of Thomson scattering to investigate a Xenon Chloride excimer laser. More specifically, the objective was to determine the electron velocity distribution of the discharge plasma as a function of time. This work follows upon the work of Elezzabi[1] who constructed the laser and studied its electron density and discharge dynamics. The electron velocity distribution is essential for comparing experimental data to theoretical modeling. Most theoretical studies have predicted a significant deviation from Maxwellian electron velocity distributions which is not found in most experimental

results. This discrepancy must be explained through more theoretical and experimental work to understand excimer laser kinetics.

To perform this experiment a short, 532 nm pulse was injected into the excimer laser and the backscattered light was analysed. The scattered beam was imaged onto the entrance slit of a spectrometer and the spectrally dispersed output was collected by either a streak camera or a photomultiplier array.

To estimate the electron temperature, it was necessary to analyse the distribution of signal intensities at shifted wavelengths. The relative timing of the probe pulse to the excimer current was needed to give a time profile of this temperature. The injection pulse power and excimer laser current were also needed to ensure that the measurement data could be normalized and therefore compared. While many attempts were made, electron temperature measurements proved to be impossible. Extremely high noise levels, an unexplained lack of resolution of the spectrometer, and possibly laser heating effects made the measurements difficult.

The only known studies of an excimer laser using Thomson scattering have been done by a Japanese group in 1989[2] and 1991.[3] The earlier experiment measured the density and electron velocity distribution for Kr/Ne, Kr/He, and Kr/Ne/HCl mixtures using a 0.85 J, 30 ns, ruby laser probe beam. These results showed a higher electron temperature for neon than for helium based mixtures. This group's later work used a frequency doubled, 0.7 J, 10 ns, Nd:YAG laser to make measurements on the same laser studied previously using a 90º scattering angle. This time measurements were also made on mixtures containing xenon; however, the xenon measurements suffered from a laser heating effect which made any results invalid. Nonetheless, for the other mixtures, an essentially Maxwellian velocity distribution was found, in disagreement with what was predicted.

The remainder of this chapter contains a brief overview of laser operation, a discussion of previous work done in this field, and a discussion of the operation of a XeCl discharge laser. The following chapters discuss, in turn, the theory of Thomson scattering,

the apparatus, the synchronization system, the measurements and results, and finally, an outline of the work that would be necessary to make this experiment successful.

1.1 Overview of Laser Operation

In this section, a brief overview of laser physics will be given since the rest of this work requires such knowledge. The principles of laser physics is more thoroughly covered in texts such as Millonni and Eberly's *Lasers*[4], or Yariv's *Quantum Electronics*[5].

As is well known, the term "laser" is an acronym for Light Amplification by the Stimulated Emission of Radiation. For the purposes of this experiment, the most useful properties of a laser are the possibilities of a narrow wavelength spectrum, high intensity, and very short pulse length.

In a simplified treatment, we can consider a medium in which electronic transitions are possible between an excited state centred around an energy E_2 and a lower state centred around an energy E_1. The upper level has a population N_2 and quantum degeneracy g_2 the lower level has a population N_1 and quantum degeneracy g_1. Interactions are possible with N_p photons of energy E_2-E_1. Photons can be absorbed by the lower level with a probability proportional to $\frac{N_1 N_p}{g_1}$; photons can be spontaneously created with a probability proportional to $\frac{N_2}{g_2}$; or photons can be emitted with the same phase and direction as existing photons with a probability proportional to $\frac{N_2 N_p}{g_2}$. This last process is known as stimulated emission. The probability for a photon at the transition frequency to stimulate emission or to be absorbed by the lower level is proportional to the number of atoms in either state. This implies that in order for there to be any amplification of incident radiation, $\frac{N_2}{g_2}$ must be greater than $\frac{N_1}{g_1}$; this condition is known as inversion. For systems in thermal equilibrium, inversions do not occur naturally as the population of any given level is given by the Boltzmann factor: $\exp(-E/k_bT)$. States with higher energies

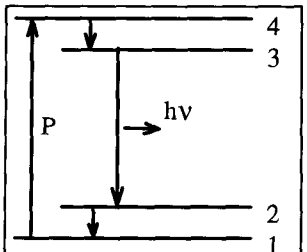

Figure (1.1) Energy Diagram for a Four Level Laser.

have less chance of being occupied. By various means inversions can be created by pumping higher level states.

Some methods to pump a medium are by focusing the radiation from flash lamps into the gain medium causing optical absorption, by passing an electrical current through the medium by transferring energy through collisions with electrons, or by combining certain chemical species which form an excited state. The rate of pumping must be sufficient to make up for the loss of excited states due to stimulated or spontaneous emission or decay.

Most practical laser mediums have more than just two levels. One of the systems we are dealing with is the four level Nd^{3+}:YAG system (see figure (1.1)). In a four level system, inversion is easily achieved if the spontaneous decay probability from 2 to 1 is greater than the probability from 3 to 2 so that the upper level will tend to be more populated in comparison when the excited atoms spontaneously cascade in energy from level 4 to 3 to 2 to 1. Also, pumping is made easier if the 4 to 3 transition is fast so that intense pumping doesn't de-excite the upper laser level. The excimer laser system will be described in more detail in the next section.

1.2.1 Laser Resonators

A resonator surrounding the gain medium is necessary to provide high intensities, to select specific modes, and to produce a narrow beam of laser light. A resonator can be formed by placing end mirrors around the gain medium. Feedback also ensures that the intensity and phase of the laser output are fairly consistent. Usually for a laser cavity, one of the mirrors is fully reflective and the other is partially reflective and lets the laser light out of the cavity. For most applications, a "stable" optical resonator is desirable. Stability implies that a group of photons reflecting between the end mirrors will repetitively pass

through the gain medium and will not be lost in the radial direction. One method to achieve this requires that at least one of the mirrors must be concave and that the distance between the mirrors must be less than the sum of the radii of curvature. For gain to occur, any losses through the mirrors or through other sources must be made up by the gain in the gain medium.

Any modes which do not match the resonance of the cavity will not be amplified.

1.2.2 Mode Locking

Short pulse production is necessary for our experiment: both to provide good time resolution as well as to efficiently produce high intensity pulses. Mode locking is used to make short pulses in the resonator. As the name suggests, mode locking refers to the technique of forcing all the longitudinal modes in a laser cavity to oscillate in phase. How this generates short pulses can easily be seen if we represent the electric field of each longitudinal mode in the laser simply as

$$E_n = E_0 \exp\left\{i\left[\omega_n\left(t-\frac{z}{c}\right)\right]+\varphi_n\right\}.$$

If the total electric field, $E_{Total,}$ is $E_{Total} = \sum_{n=-(p-1)}^{p-1} E_n$ we find that for a large number of modes of comparable strength, we need zero phase difference between the modes for there to be a pulse. We find for no phase difference between modes,

$$E_{Total} = E_0 \frac{\exp\left[ip\Delta\omega\left(t-\frac{z}{c}\right)\right]}{\exp\left[i\Delta\omega\left(t-\frac{z}{c}\right)\right]-1}$$

and $E_{Total} = 0$ otherwise. Here $\Delta\omega = \frac{c}{2L}$ and L is the cavity length. It can be shown that the shortest pulse length possible is approximately equal to 4L/pc; this is known as the Fourier limited pulse. In practice, it is usually not possible to get such short pulses from

mode locking and a technique called pulse compression is necessary to get Fourier limited pulses.

The most common way of mode locking a laser is to introduce optical losses to all modes that are not in the desired phase. The modes that have the highest round trip gain will dominate over all the others. Losses can be introduced by methods such as acousto-optic modulation.

1.2.3 Acousto-optic Modulation

Acousto-optic modulation is achieved by placing a crystal which is very efficient at promoting coupling between photons and phonons inside the optical cavity and attaching it to a piezo-electric crystal. The frequency of the driving voltage is carefully adjusted so that an acoustic standing wave is set up within the crystal. Photons passing through the cavity (with wavevector $\mathbf{k}$) have a high chance of being deflected through absorption of a phonon (with wavevector $\mathbf{k}_s$) so that $\mathbf{k} \pm \mathbf{k}_s = \mathbf{k}_{Deflected}$ as shown in figure (1.2). There will be a significant proportion of light deflected for any significant density of phonons so only the pulse traveling in resonance with the zero amplitude crossings of the acoustic wave will be amplified. Another way we can look at acousto-optic scattering is by assuming that the standing sound wave sets up a periodic variation in the refractive index. This can be described as $\Delta n(x,t) \propto \sin(k_s x)\sin(k_s t)$. The incident light will then diffract from the variations in much the same way X-rays diffract from atomic planes in crystals. This is commonly known as Bragg scattering.

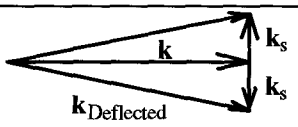

Figure (1.2) Bragg Scattering

1.2.4 Pockels Cells

Another important component in our optical system is the Pockels cell. This element allows dynamic polarization control of a polarized light beam through the use of birefringent materials and the electro-optic effect. Birefringent materials are those which exhibit different indices of refraction for different polarizations. The electro-optic effect is the variation of the degree of birefringence with an electric field.

In birefringent materials, there is a direction of propagation in crystals for which the index of refraction does not depend on the polarization known as the optic axis (OA). A wave having a polarization perpendicular to this axis will have a constant index of refraction; this is known as the ordinary wave. A wave with the orthogonal polarization and same wavevector is known as the extraordinary wave and its index of refraction depends on its direction of propagation. If we think of a light wave as being composed of two separate components of orthogonal polarizations, one polarized in the ordinary direction and the other in the extraordinary direction, the components will travel through the crystal with different velocities (due to different indices of refraction). We can see how birefringent crystals can change polarizations if we look at a linearly polarized wave, $\mathbf{E}(z,t) = \mathbf{E}_o + \mathbf{E}_{eo}$, oriented so that

$$\mathbf{E}_o(z=0,t) = \hat{i}E\sin\omega t$$

and $$\mathbf{E}_{eo}(z=0,t) = \hat{j}E\sin\omega t.$$

After traveling through the crystal a distance z_1,

$$\mathbf{E}_o(z_1,t) = \hat{i}E\sin(\omega t - k_o z_1)$$

and $$\mathbf{E}_{eo}(z_1,t) = \hat{j}E\sin(\omega t - k_{eo} z_1).$$

If $(k_{eo} - k_o)z_1 = \frac{\pi}{2}$ then the total field is circularly polarized and if $(k_{eo} - k_o)z_1 = \pi$ then the field is polarized in the orthogonal linear direction.

Combining this effect with the electro-optic effect makes dynamic control over the polarization possible. A Pockels cell contains an electro-optic crystal oriented in the

proper direction and of the proper length so that when a known voltage is provided, the desired change in polarization can be achieved. If we combine the Pockels cell with a polarizer, it is obvious that the combination can act as a switch for polarized light.

1.2.5 Second Harmonic Generation

One more component essential for our experiment is a second harmonic generator. The production of light at half the input wavelength is dependent on a non-linear electron response to an optic field. Usually, electrons in bound states are modeled to first order as being in a quadratic potential well: $V = V_0 + ar^2$. However, for the second order modeling of the anharmonic potential well, we need one more term in the potential: $V = V_0 + ar^2 + br^3$. Following Yariv, we can model the electric field forced motion of electrons in such a well as

$$\ddot{r} + \gamma r + \omega_0^2 r + Dr^2 = \frac{eE_0}{2m}\left(e^{i\omega t} + e^{-i\omega t}\right) \qquad ...(1.1)$$

with solution

$$r = \frac{1}{2}\left(q_1 e^{i\omega t} + q_2 e^{i2\omega t} + c.c.\right) \qquad ...(1.2)$$

where $q_1 = \frac{eE_0}{m}\frac{1}{\omega_0^2 - \omega^2 - i\omega\gamma}$

and $q_2 = \frac{-De^2E_0^2}{2m^2}\frac{1}{\left[\omega_0^2 - \omega^2 - i\omega\gamma\right]^2\left(\omega_0^2 - 4\omega - i2\omega\gamma\right)}$,

γ being the damping term. Therefore, it can be seen from equation (1.2) that including a second order in the approximation of the electronic potential well leads to second harmonic generation of a driving optical electric field.

The efficiency, η_{SHG}, of second harmonic generation is given to first order by

$$\eta_{SHG} = \frac{P_{2\omega}}{P_\omega} = \frac{\sin^2\left(\frac{\Delta kL}{2}\right)}{\left(\frac{\Delta kL}{2}\right)^2} \qquad ...(1.3)$$

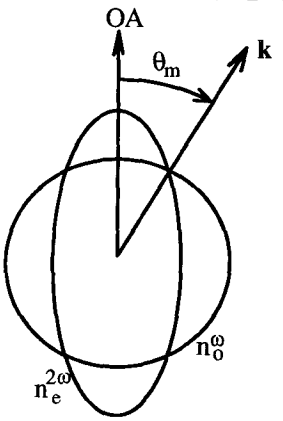

Figure (1.3) Second Harmonic Generation Index Matching: Indices of Refraction for a Negative Uniaxial Crystal

where $\Delta k = k^{2\omega} - 2k^{\omega}$. For maximum efficiency, we want this phase difference to approach zero. Intuitively, we can see why this is necessary. Knowing that the second harmonic wave is generated in phase with the pumping wave, if there is no phase matching then the second harmonic generated at one point will interfere with the second harmonic generated at all other points. The most common method for phase matching, in appropriate crystals, is to send in the pump wave polarized on the ordinary axis and generate the second harmonic polarized on the extraordinary axis. The angle of the direction of propagation with respect to the optic axis has to be carefully chosen so that the phase matching condition is fulfilled. Figure (1.3) illustrates this condition for a negative uniaxial crystal (a crystal that has only one optic axis and where $n_e < n_o$). This condition can be described mathematically as

$$\sin^2\theta_m = \frac{n_o(\omega)^{-2} - n_o(2\omega)^{-2}}{-\left[n_o(\omega)^{-2} - n_e(2\omega)^{-2}\right]}.$$

Small deviations from the phase matching condition can lead to dramatic losses in the conversion efficiency. So precise control of the orientation is necessary.

The efficiency implied by equation (1.3) is in fact not achievable. The theory used to derive this equation assumes that the intensity of the beam at ω does not change with distance; but energy must of course be taken from the pump beam and put into the second harmonic. The theoretical maximum conversion efficiency does indeed approach 100% with very high intensities but the damage threshold of real crystals is below the necessary intensities.

1.2 Historical Overview

The electron temperature of a plasma can be determined by various spectroscopic methods[6] or by Thomson scattering. Thomson scattering, the scattering of radiation from free electrons, first was used to study the ionosphere using radio waves. The advent of lasers in the early 60's provided the necessary powerful, monochromatic light sources needed to perform such scattering in a laboratory. The very first studies were done by Fiocco and Thompson;[7] they studied light scattering from an electron beam. This work was quickly followed by many studies of laboratory plasmas: for example see Thompson and Fiocco[8].

The first excimer lasers were developed around 1972. Excimer lasers are of interest to science and industry because of their high gain, high efficiency, and high power at ultraviolet wavelengths. They have high gains since the lasing transition has a thermally unstable ground state. This means that there is little absorption at the lasing frequency because there are very few molecules in the lower laser level. Many excimer laser systems have been found; they can be divided into classes such as rare gas, rare gas halogen, metal vapor, or triatomic rare gas excimers[9]. The type we are interested in are the rare gas halide excimers.

Quickly following the announcements of the potential of rare gas monohalide systems as laser media[10,11], the first such lasers appeared in 1975[12,13,14]. They used electron beams to produce the necessary excitation. To make electrical discharge pumping feasible, first the obstacle of inherent discharge instability in excimer systems had to be overcome. This was done by developing the preionization process to create a relatively uniform distribution of electrons prior to the main discharge and developing low-impedance circuits to make very fast discharges possible. The first transverse discharge excimer lasers appeared in 1976 and 1977[15,16,17,18]. Electron beam pumping is still popular due to the high lasing efficiency achievable but discharge pumping is more convenient to use due to

the smaller size, simpler operation, and lower cost. A further possibility is the use of an electron beam to stabilize a transverse discharge[19]; however, this will not be discussed further here.

1.3 XeCl Laser Chemistry and Kinetics

In step with the development of laboratory excimer lasers was the development of theoretical modeling of these systems. Excimer systems are very complex due to the large number of chemical species present. They are difficult to model because often over 50 rate equations are needed and many of the rate constants are not known accurately. Nonetheless, results that agree well with experiment can be obtained[20]. Most of the understanding of excimer chemistry is derived from theoretical modeling.

As mentioned earlier, the XeCl laser chemistry is fairly complex. The ground state corresponds to a ^1S rare gas atom covalently bonded to a ^2P halogen atom. The weakly bound state is known as the X state and acts as the lower laser level. The upper laser level is an ionicly bonded molecule consisting of a ^2P state rare gas atom as the donor and a ^1S halogen as the acceptor. This is known as the B state; this molecule is known as an excited dimer - hence the term "excimer" from the contraction.

In the gas mixture are small amounts of the rare gas and the halogen donor. The majority is a buffer gas such as helium or neon. In early XeCl systems Cl_2 was used as the chlorine donor; however, due to absorption at the laser wavelength by Cl_2, efficiencies were improved when HCl was used instead. The active rare gas (krypton or xenon) can absorb energy directly from the discharge; however, a buffer gas is necessary to prevent the glow discharge from becoming unstable. The light buffer gas molecules efficiently absorb energy from the accelerated electrons through elastic collisions and can transfer their energy to the active species easily through Penning ionization or associative ionization.[21] Helium is a good buffer gas; because of its low mass, it most efficiently

absorbs the electron energy. Other buffer gasses such as neon have a greater tendency to allow arcing due to its lower discharge impedance: less than half of that of helium.[22] Nonetheless, in many cases it might be preferable to use neon over helium because of the greater lasing efficiencies possible[20].

The formation of $XeCl^*$ molecules can be summarized in figure (1.4). Depicted in this diagram are the dominant pathways for the formation of the excimer. It can be seen that there are at least two steps for the formation of XeCl*. Firstly, the excited or ionized xenon atom has to be formed, collisionally with electrons or through Penning ionization by a metastable He^* atom:

$$Xe + e^- \rightarrow Xe^* + e^- \qquad (1.4)$$

or

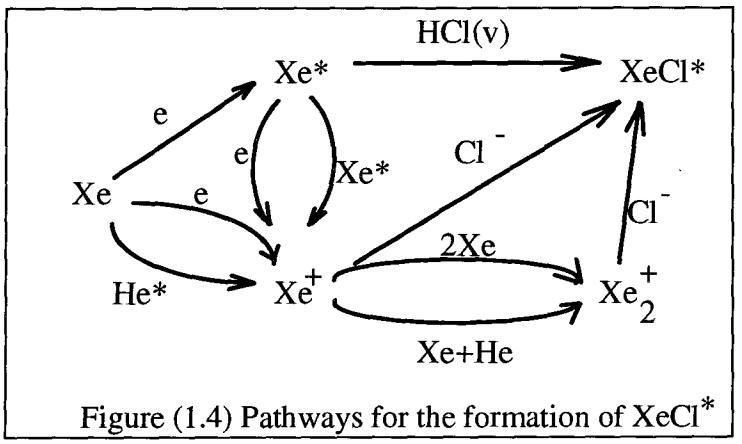

Figure (1.4) Pathways for the formation of $XeCl^*$

$$Xe(\text{or } Xe^*) + e^- \rightarrow Xe^+ + 2e^- \qquad (1.5)$$

or

$$Xe + He^* \rightarrow Xe^+ + He^- + e. \qquad (1.6)$$

In this step, the electron distribution function is very important. Electrons gain their energy directly from the electric field between the electrodes. The electrons undergo elastic collisions until they reach the ionization potential or the first excitation energy of one of the gas elements. They then loose their energy through an inelastic collision. The

metastable excited states play a large part in these excitation processes because of their large cross sections and high concentrations.

After the xenon atom is excited to a metastable state or ionized, the excimer can be formed through three pathways. The first involves a reaction with the excited HCl molecule,

$$Xe^* + HCl(v) \rightarrow XeCl^* + H, \qquad (1.7)$$

the second by ion- ion recombination with Cl^-,

$$Xe^+ + Cl^- + X \rightarrow XeCl^* + X, \qquad (1.8)$$

or the third in two steps,

$$Xe^+ + 2Xe \rightarrow Xe_2^+ + Xe \qquad (1.9)$$

or

$$Xe^+ + Xe + He \rightarrow Xe_2^+ + He \qquad (1.10)$$

then

$$Xe_2^+ + Cl^- \rightarrow XeCl^* + Xe. \qquad (1.11)$$

In reactions (1.8) to (1.10) it can be seen that a third, neutral atom, is required to remove excess kinetic energy from a newly formed molecule.

These reactions have been studied a great deal through computer modeling. In order to model the excimer discharge, tables of collision cross sections are needed. These are tabulated in many sources as for example by Maeda *et al.*[21] For the calculation of electron excitation or ionization rates, it is necessary to calculate the electron velocity distribution by finding a self consistent solution to the Boltzmann equation: $\frac{\partial f}{\partial t} + \mathbf{v} \cdot \frac{\partial f}{\partial \mathbf{r}} + \mathbf{a} \cdot \frac{\partial f}{\partial \mathbf{v}} = \left(\frac{\partial f}{\partial t} \right)_{collision}$. The rates for ion-ion recombination can be determined by Flannery's equation[23] which utilises quasi-equilibrium statistics.

It can be seen from equations (1.8) and (1.11) that the rate of formation of Cl^- is essential to the efficient operation of the XeCl system since it controls the rate of

formation of the excited dimer. Cl^- production occurs through the electron attachment reaction,

$$HCl + e \rightarrow H + Cl^-. \quad ...(1.12)$$

This reaction limits the pulse duration since the HCl is not regenerated in the time scale of the pulse. Other factors prevent one from simply increasing the concentration of HCl to provide sufficient Cl^- atoms[25].

The role of HCl in the onset of arcing can also be seen. Arcing is thought to start with a HCl local density less than the average for the system. Since the electron attachment reaction (equation (1.12)) is the primary mechanism for electron loss, a paucity of HCl means that the density of electrons will increase over the average. This increase reduces the local resistivity causing more current to flow locally thereby increasing ionization. In this way a positive feedback loop is established which triggers arcing[24]. This also indicates the importance of uniform preionization so that this feedback loop is not started.

2 Theory

All discussions in this thesis will utilize the rationalized MKS system of units.

2.1 Definition of Electron Temperature

For a system of particles in equilibrium, undergoing elastic collisions, a temperature can be defined by the expected Maxwellian velocity distribution, $f_0(\mathrm{v})$,

$$f_0(\mathrm{v}) = \exp\left(-\frac{\mathrm{v}^2}{a^2}\right)(\pi a^2)^{-\frac{3}{2}}, \qquad ...(2.1)$$

or

$$f_0(\mathrm{v}) = \exp\left(-\frac{m\mathrm{v}^2}{k_B T}\right)\left(\frac{2\pi k_B T}{m}\right)^{-\frac{1}{2}}, \qquad ...(2.2)$$

where v is the particle speed, it is the mean thermal speed, and T is the defined temperature. Due to the large mass difference between electrons and ions, the electron-ion momentum transfer cross section is very small. This means that the different species in the plasma can have different effective temperatures for short time periods.

The effects of inelastic and superelastic (where an excited species is de-excited by the collision) collisions will make the distributions non-Maxwellian. This effect has been shown in many theoretical studies[20] but has been shown to be less important in experimental studies[3,20] of excimer laser systems.

2.2 Thomson Scattering

The theory of Thomson scattering has been comprehensively outlined in Sheffield[25], only a brief outline of the relevant points will be presented here. In this derivation, we are trying to find the wavelength distribution of monochromatic light scattered from the electrons in a plasma. To do this we will first find the radiation emitted by an electron

accelerated to a low velocity. Then we will assume that the charges are being accelerated by the probe laser beam. Lastly we will find the effects of electron correlations and the electron distribution function on the scattered spectrum.

Taking Maxwell's equations and combining we get,

$$\nabla\times(\nabla\times\mathbf{E})+\frac{1}{c^2}\frac{\partial^2\mathbf{E}_i}{\partial t^2}=-\mu_0\frac{\partial\mathbf{J}}{\partial t}. \qquad ...(2.3)$$

If we take **J** to be the motion of single charges

$$\mathbf{J}=q\mathbf{v}(t'), \qquad ...(2.4)$$

where t' is the retarded time given by

$$t'=t-\left(\frac{R'}{c}\right). \qquad ...(2.5)$$

and R' is the distance from the charge to the observer at time t'.

Solving equation (3) we get

$$\mathbf{E}(R',t)=\frac{q}{4\pi\varepsilon_0}\left[\frac{(\hat{s}-\beta(t'))(1-\beta^2(t'))}{(1-\hat{s}\cdot\beta(t'))^3R'^2}\right]+\frac{q}{4\pi\varepsilon_0 c}\left[\frac{\hat{s}\times\{(\hat{s}-\beta(t'))\times\dot{\beta}\}}{(1-\hat{s}\cdot\beta(t'))^3R'}\right] \qquad ...(2.6)$$

where $\beta\equiv\frac{\mathbf{v}}{c}$ and $\hat{s}$ is the unit vector from the charge to the observer (see figure (2.1)).

For a low velocity charge, where $\beta<<1$, equation (2.6) reduces to

$$\mathbf{E}(R,t)=\frac{q}{4\pi\varepsilon_0 cR}\left(\hat{s}\times(\hat{s}\times\dot{\beta}(t)\right). \qquad ...(2.7)$$

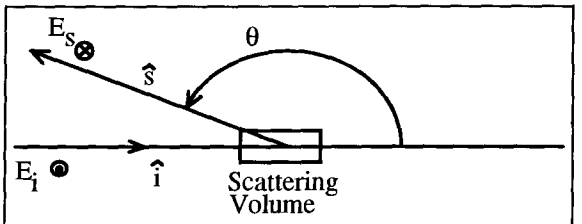

Figure (2.1) Scattering Definitions

Assuming that the incident radiation can be described as

$$\mathbf{E}_i=\mathbf{E}_0\cos(\mathbf{k}\cdot\mathbf{r}-\omega_i t) \qquad ...(2.8)$$

and the position of the charge can be described as

$$\mathbf{r}(t')=\mathbf{r}(0)+\mathbf{v}t', \qquad ...(2.9)$$

solving the equation of motion for an electron in the absence of a magnetic field, $m\dot{\mathbf{v}} = q\mathbf{E}_i$, and substituting into equation (2.7) gives the scattered electric field,

$$\mathbf{E}_s(\mathbf{R},t) = \frac{q}{4\pi\,\varepsilon_0 cmR}\left[\hat{s}\times(\hat{s}\times\mathbf{E}_{i0})\right]\cos\left[\mathbf{k}_s\cdot\mathbf{R}-\omega_s t-(\mathbf{k}_s-\mathbf{k}_i)\cdot\mathbf{r}(0)\right], \quad ...(2.10)$$

where $\omega_s = \omega_i\frac{(1-\hat{i}\cdot\beta)}{(1-\hat{s}\cdot\beta)}$ is the Doppler shifted frequency and $\hat{i}$ is the unit vector in the direction of the probe beam propagation. It should be noted here that because of the mass term in the denominator, scattering from ions can generally be neglected. The scattered wavenumber and frequency can also be found from the usual conservation of energy and momentum arguments: $\pm\omega_s = \omega_e + \omega_i$ and $\pm k_s = k_e + k_i$. In the case we are interested in, $\hat{s}$ and $\mathbf{E}_{i0}$ are orthogonal therefore the $\left[\hat{s}\times(\hat{s}\times\mathbf{E}_{i0})\right]$ term becomes -$\mathbf{E}_{i0}$.

Given the radiated electric field from one electron, we can find the total radiated power simply by taking the vector sum of the contribution from each electron.

$$\frac{dP_s}{d\Omega} = \varepsilon_0 c^2 R^2 \left(\sum_{j=1}^{N}\mathbf{E}_{js}\sum_{l=1}^{N}\mathbf{E}_{ls}\right) \quad ...(2.11)$$

which can be written as

$$\frac{dP_s}{d\Omega} = \varepsilon_0 c^2 R^2\left[NE_s^2 + N(N-1)(\mathbf{E}_j\cdot\mathbf{E}_l)_{j\neq l}\right] \quad ...(2.12)$$

where N is the number of electrons in the scattering volume. Obviously, the first term is the power from individual electrons and the second term is the power from correlations of electrons.

The Debye length, λ_D, is a very important parameter for plasma physics because it is the distance over which charges will act collectively. At distances greater than the Debye length, the relatively long range Coulomb interaction can be neglected due to shielding by surrounding charges. If we are irradiating the plasma with a light beam that has a wavelength that is much smaller than the Debye length then any correlations between the electrons will not be apparent since the electrons are seen individually. $\lambda_D = \left(\frac{\varepsilon T}{e^2 n_e}\right)^{1/2}$

where ε is the dielectric constant and n_e is the electron density.

A useful parameter is $\alpha \equiv (k\lambda_D)^{-1}$. For incoherent scattering, $\alpha << 1$ and scattering is from individual electrons. In our case, we have $n_e = 3 \times 10^{15}\,\text{cm}^{-3}$, $T_e = 2$ eV, $\theta = 179.5°$, $\lambda = 532$ nm which gives an α of 0.22: definitely incoherent scattering. In further discussions, we will neglect the second term of equation (2.12) so the power is just the sum of the powers from the individual electrons.

From an experimental point of view, we are interested in radiation scattered in a certain frequency range through a certain solid angle for the entire scattering volume

$$\frac{dP_s}{d\Omega} = \frac{\varepsilon_0 c^2 R^2 N}{2} \int d\mathbf{v} f(\mathbf{v}) E_s^2(\mathbf{R},t) \delta(\omega_s - \omega_i - \mathbf{v}\cdot\mathbf{k}). \qquad ...(2.13)$$

The E_s^2 term can be brought out of the integral and the equation rearranged so that

$$P_s\, d\omega\, d\Omega = \left(\frac{q}{4\pi\,\varepsilon_0 cm}\right)^2 N E_{i0}^2 \int d\mathbf{v}\, f(\mathbf{v}) \delta(\omega_s - \omega_i - \mathbf{v}\cdot\mathbf{k}) d\omega_s\, d\Omega \qquad ...(2.14)$$

followed by

$$P_s\, d\omega_s\, d\Omega = N\left(\frac{q}{4\pi\,\varepsilon_0 cm}\right)^2 E_{i0}^2 f\left(\frac{\omega}{k}\right)\frac{d\omega_s}{k} d\Omega. \qquad ...(2.15)$$

This means that the reflected power at a given wavelength is simply proportional to the corresponding velocity distribution. Knowing that the classical electron radius, r_0 is $\frac{q}{4\pi\varepsilon_0 mc^2}$, and assuming a Maxwellian velocity distribution,

$$P_s\, d\omega_s\, d\Omega = P_{i0} r_0^2 n_e L \exp\left(-\frac{\omega^2}{k^2 a^2}\right)\left(\pi k a^2\right)^{-3/2} d\omega_s\, d\Omega \qquad ...(2.16)$$

Since $\mathbf{k} = \mathbf{k}_s \pm \mathbf{k}_i$, by the cosine rule, $k^2 = k_s^2 + k_i^2 - 2k_s k_i \cos\theta$ where θ is the scattering angle. If we assume that $\frac{v}{c} << 1$ then $k^2 = -2k_i \cos\theta$ and $\left(\frac{\omega}{ka}\right)^2 \cong \frac{c^2 \Delta\lambda^2}{4a^2\lambda_i^2 \sin^2\left(\frac{\theta}{2}\right)}$. Putting this into terms that we can relate to experimentally,

$$P_s(R,\lambda_s)\, d\lambda_s\, d\Omega = \frac{P_i r_0 n_e L\, c\, d\Omega}{2\pi^{1/2} a \sin\left(\frac{\theta}{2}\right)} E_{i0}^2 \exp\left(\frac{c^2 \Delta\lambda^2}{4a^2\lambda_i^2 \sin^2\left(\frac{\theta}{2}\right)}\right)\frac{d\lambda_s}{\lambda_s} \qquad ...(2.17)$$

Taking the logarithm of both sides, we can easily see that if ln P_s is plotted against $\Delta\lambda^2$ then the slope would be $\frac{c^2}{4a^2\lambda_i^2 \sin^2\left(\frac{\theta}{2}\right)}$ **or** $\frac{c^2 m_e}{8k_B T_e \lambda_i^2 \sin\left(\frac{\theta}{2}\right)}$ and the electron temperature can be readily obtained from the slope.

[25]J. Sheffield, *Plasma Scattering of Electromagnetic Radiation* (Academic, New York, 1975).

3 Apparatus and Setup

The contents of this chapter will be confined to a physical description of the apparatus with very few details of the electronics. The following chapter will describe the precise synchronization of the components.

3.1 Overview

An overview of the apparatus is depicted in figure (3.1). The short seed pulse is produced in the Spectra Physics oscillator and amplified by the Continuum Regenerative Amplifier, injected through the excimer laser, and absorbed by a beam dump. The light scattered from the excimer discharge volume is collected with a large lens, spectrally dispersed in the spectrometer, measured, and analysed.

3.2 Excimer Laser

The excimer laser in this experiment was constructed by Elezzabi for his M.Sc. thesis[1]. The description of this laser will be divided into sections discussing, in turn, the laser body, the circuitry, and the operation.

3.2.1 Excimer Laser Body Construction

The glow discharge takes place between two parallel brass electrodes with a modified Chang profile[26], 35 cm long with a 1.5 cm gap. For the experiments, the chamber was filled with a 5.3 atm mixture: [He]:[Xe]:[HCl] = 99.63 : 0.12 : 0.25. The charging voltage of the system was between 15 and 22 kV and the operating pressures were between 3.1 and 5.6 atm. To reduce optical losses, the end windows were set at the Brewster angle (θ_B = 57.1°) for the UV light at 308 nm: the excimer lasing

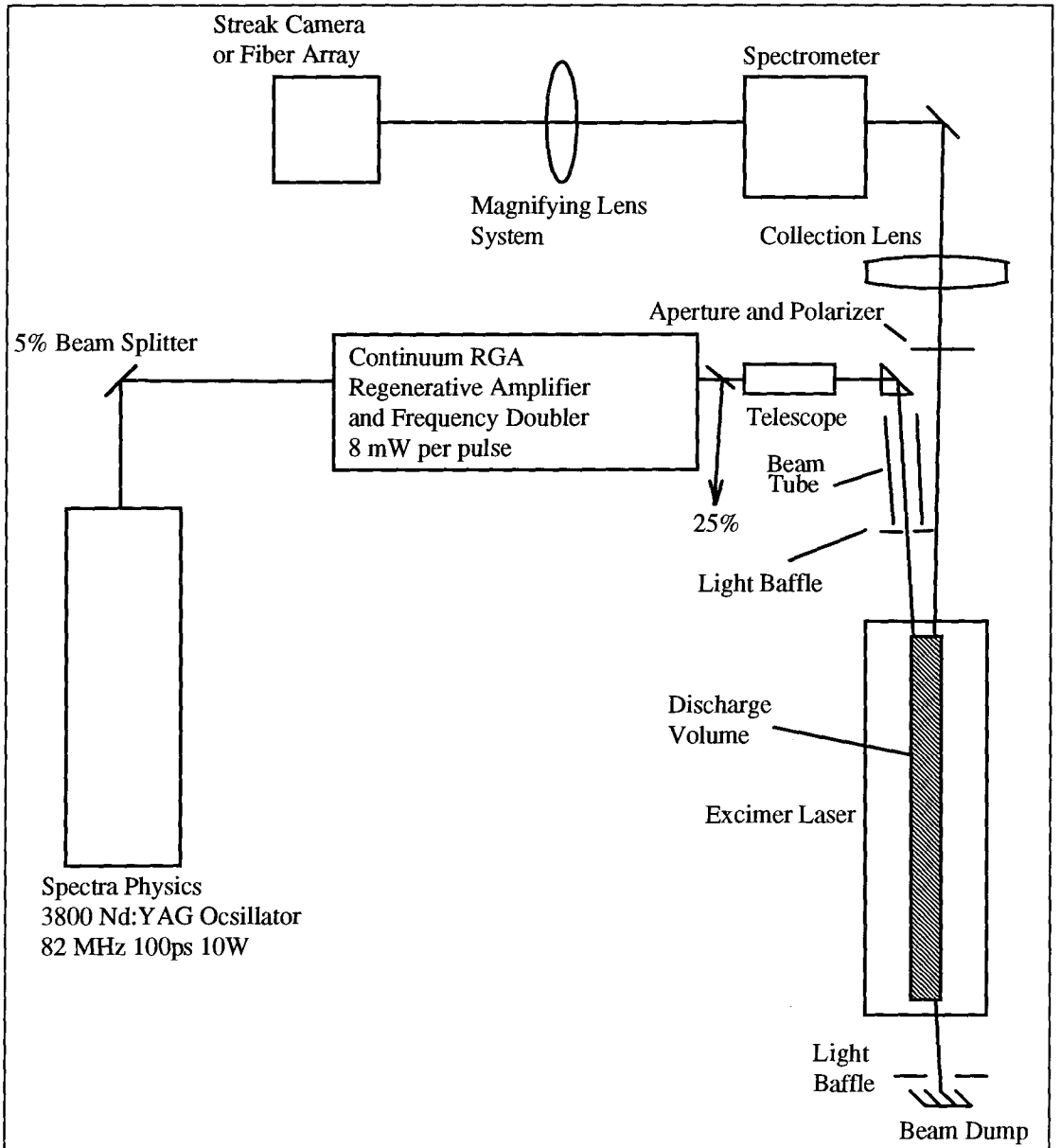

Figure (3.1) Experimental Setup

wavelength. It was estimated that the glow discharge was approximately 0.5 cm wide, giving a discharge volume of approximately 26.25 cm^3.

The gas was preionized by two rows of spark preionizers, placed half-way between and to the sides of the two electrodes (see figure (3.2)). The preionizers were made by fitting 17, 2.5 cm long stainless steel tubes on a 5 mm diameter glass rod. The ends of the tubes were cut at 30° and spaced 1 mm apart so that when a large potential

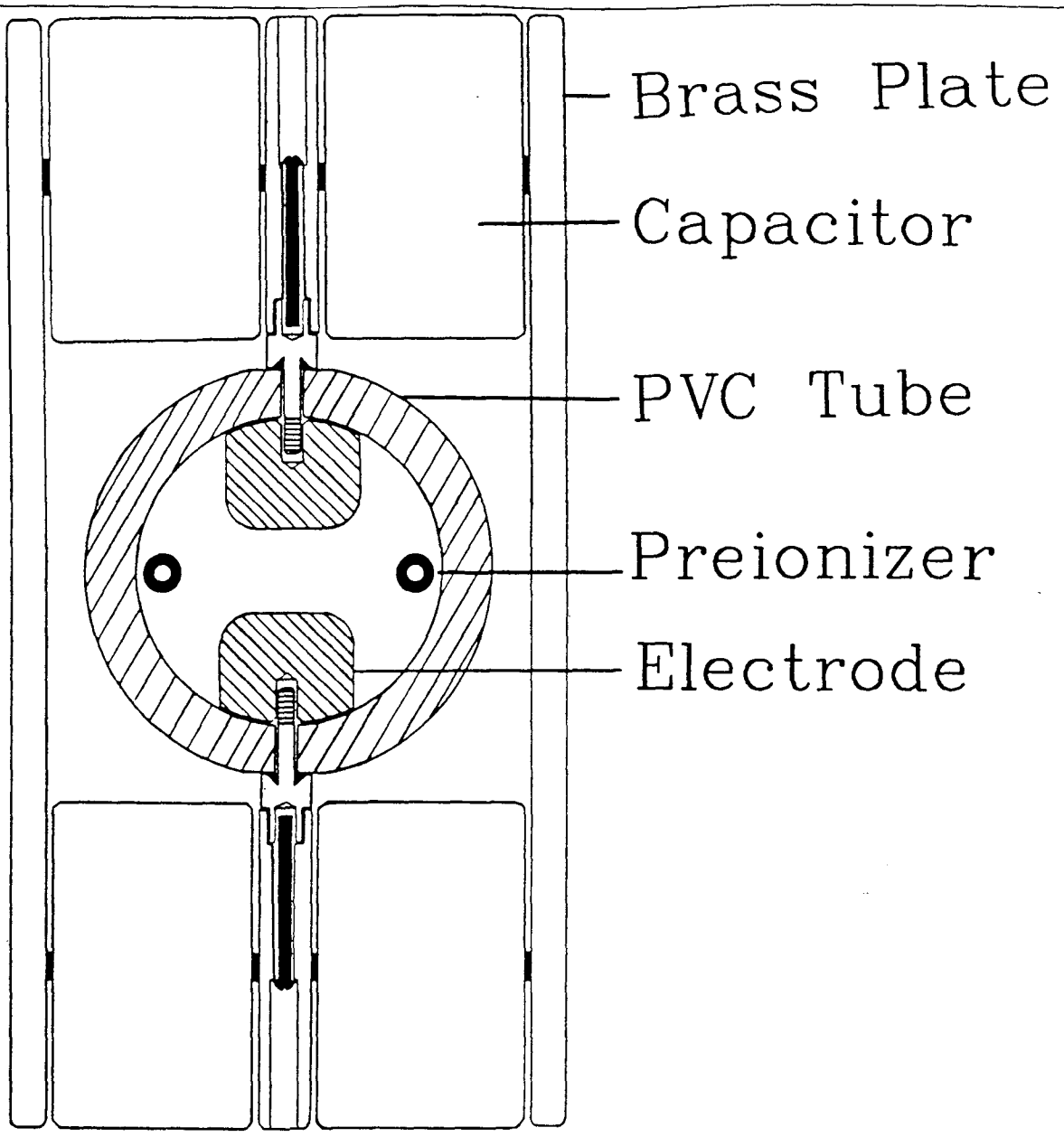

Figure (3.2) Cross Section of Laser Body

difference was applied to the ends, sparks would appear at each of the gaps. Many of the high energy photons produced in the sparks would be absorbed in an ionizing gas atom transition. This provided the necessary free electrons to enable a uniform discharge. It was roughly estimated that such preionization produced an initial electron density of 10^7 cm^{-3}.

The laser was enclosed in a grounded fine copper mesh to reduce radio frequency noise produced by the discharges.

When this system was operated as a laser, a 100% reflecting mirror would be placed at one end of the cavity and a quartz flat would be placed at the other. The mirror and the flat would then be aligned using a HeNe laser.

3.2.2 Excimer Laser Circuit

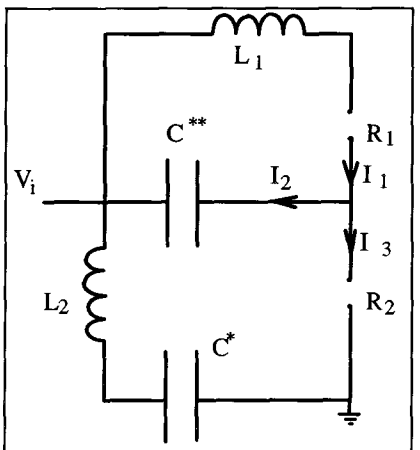

Figure (3.3) Simplified Laser Discharge Circuit

As mentioned earlier, a fast discharge circuit is necessary to avoid arcing in the discharge. For this excimer laser, a LC double inversion circuit is used. This circuit has the advantage of requiring only one spark gap and a power source supplying only one polarity. This increases the reliability and reduces the timing jitter of the circuit. This is also a relatively fast circuit compared to other high speed discharge circuits[27].

A diagram of half the circuit is shown in figure (3.3). Here, R_1 is the spark gap, R_2 is the main discharge volume, L_1 is the circuit inductance and L_2 is the laser head inductance. C^* and C^{**} are the energy storage capacitors. When the spark gap (R_1) is triggered, current flows from the capacitors through the inductance and spark gap until the voltage across the main discharge (R_2) is greater than the breakdown potential of the gas. Then the main gap breaks down and current I_3 starts to flow. The inductance L_1 from figure (3.3) is simply the loop inductance: calculated to be 27 nH. The discharge resistance (R_2) varies with operating conditions but has been found to be in the order of 0.5 Ω.

A complete electronic diagram, including the preionization circuit, is shown in figure (3.4). It can be seen that the preionizers are capacitively coupled to the main circuit. This prevents sparking from the main electrodes to the preionizers by keeping the voltage of the preionizers halfway between the electrode voltages. The preionizer capacitance was provided by two, 2.7 nF capacitors in parallel for each preionization rod.

To minimize the circuit inductance, the 24, 2.7 nF doorknob capacitors are divided into four equal groups as shown in figure (3.4). The high voltage sides are

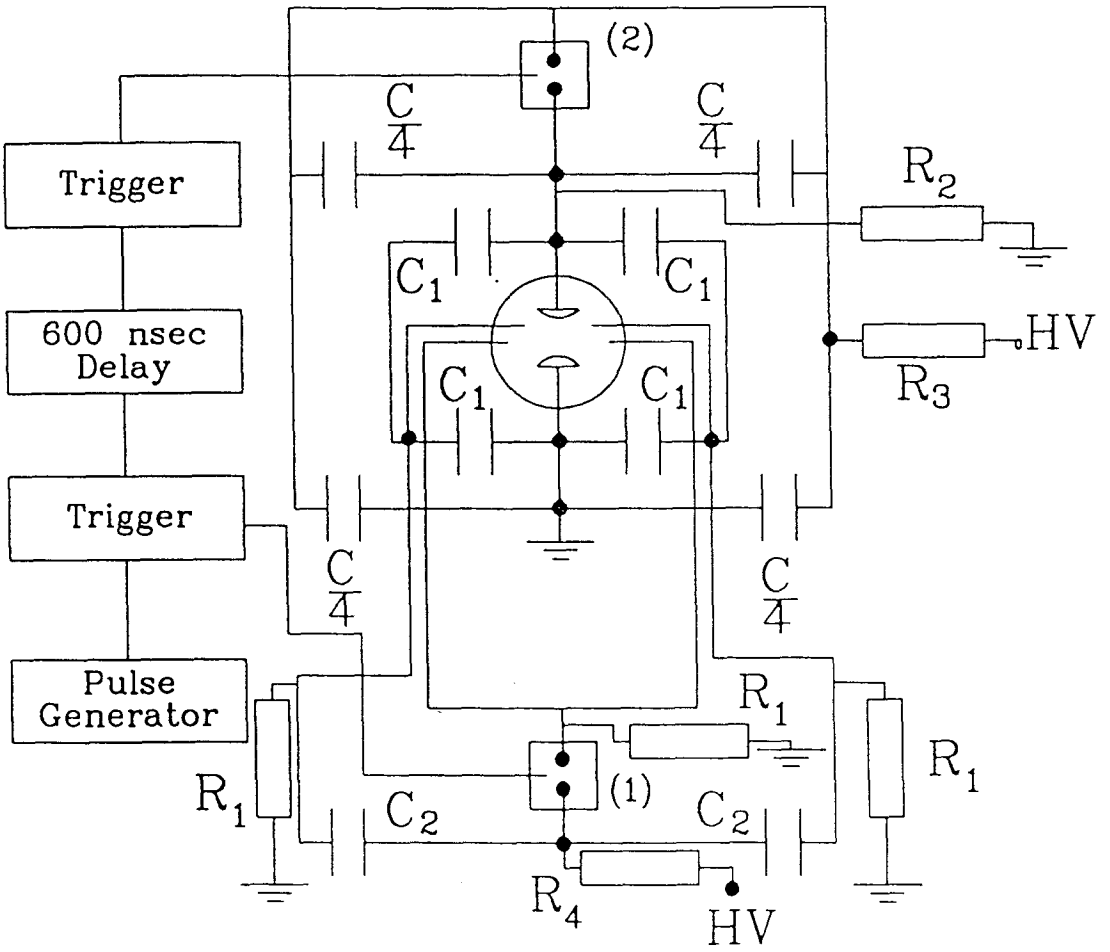

Figure (3.4) Laser Circuit

connected to two large brass plates (21.1 cm × 33.2 cm × 0.65 cm).

The spark gap electrodes are made of brass mounted in a Lucite chamber. The discharge was triggered by a -10 kV trigger pulse to a triggering pin located at the centre of the cathode. This pulse was formed by a 4:1 step up transformer and a EG&G Krytron unit. Pressurized dry air flowed through the spark gaps to control the breakdown voltage and to remove ozone. The air pressures and flow rates were controlled by manipulation of the air bottle regulators and small valves contained in the air exhaust lines.

3.2.3 Excimer Laser Operation

With careful adjustments of the spark gap pressures and the voltage, the discharge jitter of the excimer laser could be kept under 5 ns. In other words, the standard deviation of the time differences between the trigger pulse and the establishment of the discharge in the excimer was less than 5 ns. Usually such a low jitter was not necessary. It was easiest to take measurements over the entire pulse (≈60 ns) not by precise variation of the relative timing of the injection laser pulses, but by letting the natural variation in timing randomly sample the pulse with each shot.

The quality of the glow discharge could be monitored visually through a Plexiglas sheet which filtered out ultraviolet light; any arcing would be readily apparent due to its brightness in relation to the glow discharge. Arcing was also easily detected by the irregular current signal that it produced.

To stop persistent arcing a sequence of procedures was followed until the arcing disappeared. Firstly, the spark gap pressures would be lowered until the pressure was just high enough to prevent a breakdown; secondly, the excimer body would be evacuated for a number of hours in an attempt to remove any impurities present and then the cavity would be refilled with fresh gas; thirdly, if the previous steps didn't

work, the chamber would be filled with helium and the electrodes would be conditioned by using a function generator to repetitively trigger discharges for a number of hours; as a last resort, the electrodes would be manually cleaned and the system would be carefully examined for any air leaks.

The gas recovery time for this laser was approximately 30 s. Any attempts at increasing the repetition rate would, after a few shots, result in increased jitter and greater chance of arcing. The gas mixture would have to be replaced every one or two days due a buildup of the gas impurities.

3.3 Injection Pulse Production

The probe pulse was produced by amplifying 5% of a ≈100 ps ≈100 nJ pulse from a Spectra Physics model 3800 Nd:YAG (Nd^{3+} doped Yttrium Aluminum Garnet) laser with a Continuum RGA regenerative amplifier.

3.3.1 Nd:YAG Oscillator

The laser oscillator utilized a Nd:YAG rod in the centre of a symmetrical 1.8 m long cavity. The mode was controllable by a series of removable, 0.8 to 1.5 mm, apertures placed near the YAG rod. The quartz acousto-optic mode locker was placed inside the cavity near the output coupler. The acoustic driving frequency was approximately 41.1 MHz. The resultant pulse frequency was 82.2 MHz with a pulse length of approximately 100 ps. We didn't have the necessary apparatus to measure the pulse length more accurately. The average output power was approximately 12 W. A dielectric beamsplitter was used to split off 5% of this beam to be amplified in the regenerative amplifier.

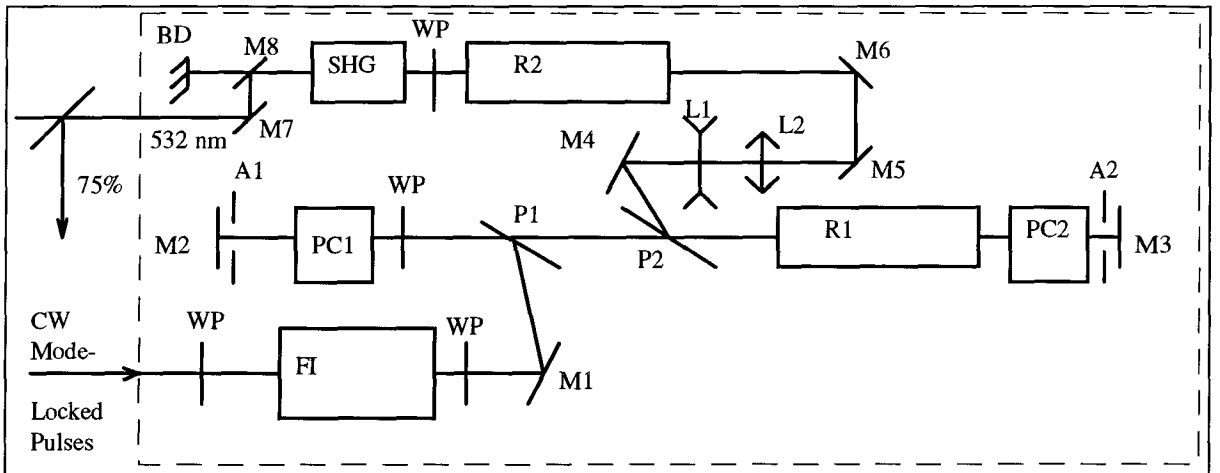

M1 to M7 - 100% Mirrors
M8 - 532 nm Dielectric Mirror
P1, P2 - Dielectric Polarizers
SHG - Second Harmonic Generator
L1 - Diverging lens, -92 mm
L2 - Converging lens 155 mm
A1- 0.65 mm Aperture
A2 - 3.5 mm Soft Aperture
WP- Half Wave Plates
BD - Beam Dump
R1 - Nd:YAG Amplifier Rod 6 mm diameter, 115 mm long
R2 - Nd:YAG Amplifier Rod 9 mm diameter, 115 mm long

Figure (3.5) Diagram of the Regenerative Amplifier

3.3.2 Regenerative Amplifier

In a regenerative amplifier, a seed laser pulse is switched into a cavity, makes multiple passes through the gain medium, each time along the same path, and is switched out. The layout of this regenerative amplifier is shown in figure (3.5).

The pulse train was accepted into the regenerative amplifier through a Faraday isolator which prevented any feedback into the oscillator. At the mirror M1, the pulse has a vertical polarization. It can be seen that if the Pockels cell has no applied voltage, the two passes through the following half wave plate will cause the vertically polarized pulse to be rejected by the polarizer P1. However, if the Pockels cell rotates the polarization such that after two passes it has rotated into the horizontal direction and the wave plate rotates it into the orthogonal polarization, the pulse will be accepted into the cavity.

At appropriate times the first Pockels cell was switched on and quickly off so that a single pulse would be accepted into the amplifier cavity. The pulse was then amplified with each pass through the YAG rod until the gain medium was depleted. The pulse was then switched out by the second Pockels cell and sent through an additional single pass Nd:YAG amplifier and a frequency doubling KDP (Potassium Dihydrogen Phosphate: KH_2PO_4) crystal. A dielectric mirror was used to separate the 532 nm light from the residual 1064 nm light. The 1064 nm beam was directed into a beam dump since it was not needed. Green light pulses of up to 90 mJ could be produced at 10 Hz. The power was measured using a Scientech Model 380101 Energy Detector. This detector had an integration time of over 10 sec, which made the measurement of single pulses impossible. 25% of this beam was removed from the total beam using a dichroic beamsplitter and was used for other purposes.

It should be mentioned that the power actually used for Thomson scattering was considerably less than 75% of 90 mJ per shot for two reasons. Firstly, as will be described later, the laser was operated in "fixed" mode giving a less than optimum output power: estimated to be 70 mJ per shot. Secondly, a significant proportion of the probe beam was lost in reflections and by absorption. The energy reaching the discharge was approximately 40 mJ per pulse. Unfortunately, we didn't have equipment to conveniently measure the energy of a single pulse so visual estimates had to be made using comparisons to the full power pulses on Kodak burn paper.

The quarter wave voltages for the Pockels cells were applied by two Marx banks. Each consisted of a series of capacitors in parallel which were charged up to 300 V. When the "fire" signal was sent to the Marx bank, the terminals were electronically reversed so that the capacitors were in series and 2700 V was provided across the end terminals with a rise time of less than 1 ns.

3.3.3 Steering Optics

To inject the beam into the excimer laser and produce the required beam size, the laser light was passed through a telescope made by two lenses: the first of focal length 433 mm and the second of 127 mm. To avoid creating an air spark (an electrical breakdown due to a high optical electric field), the focal point was enclosed by a small vacuum chamber as shown in figure (3.6).

The second telescope lens was adjusted so that the beam entering the plasma was collimated with a diameter of approximately 4 mm. This diameter was necessary as it was suspected that a smaller one would create electric fields large enough to create a gas breakdown in the laser discharge volume which would give false measurements for the experiment.

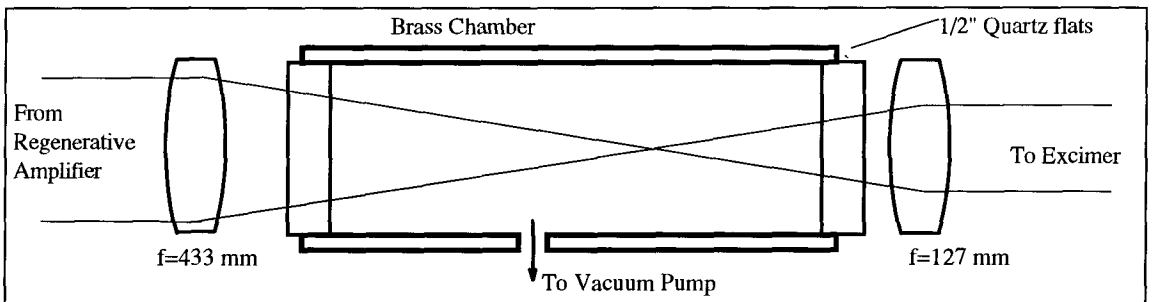

Figure (3.6) Telescope Arrangement for Injected Pulse

All beam steering was done with prisms as it was found that any metal coated mirrors would be damaged. Careful alignment was necessary to ensure good beam quality in the plasma.

3.4 Collection Optics

The back scattered light was picked up by a large, 307 mm anti-reflection coated lens with an f number of f/2.5 (the f number is defined as the ratio of the focal length to the aperture diameter). The lens was positioned so that the scattering angle was

179.5°. A field stop aperture and a vertical polarizer was placed directly in front of the lens. The aperture was usually opened to 24 mm. The function of the polarizer was to attenuate diffusely scattered light. This would improve the signal to noise ratio since any Thomson scattered light would be vertically polarized.

The collected signal was imaged onto the entrance slit of a f/3.6 Jarrel-Ash 82-410 0.25 meter Ebert Monochromater with the exit slit removed to create a spectrometer. The dispersed signal was then magnified as necessary and imaged onto the entrance slit of the streak camera array or the face of the array of fibre bundles which passed the signal through the walls of the screened room to the photomultipliers.

Various precautions were taken to reduce stray light. To minimize light reflected from the laser body and electrodes, the beam was passed through a metal mask with a 4 mm circular hole just before it was injected into the plasma. To ensure that the light scattered from the mask was not picked up by the collection lens, the beam path from the last prism to the mask was enclosed in a beam tube: a length of PVC tube painted black. After passing through the scattering volume the beam was directed into a stack of razor blades painted black[28]. This beam dump was designed to absorb the incident laser beam with as little reflection as possible and to provide an optically black background for the collection optics. It was placed about a meter behind the exit window of the excimer and behind another light baffle in order to minimize any light scattered from objects behind the laser.

The field stop aperture was taped to the front of the collection lens. The lens, entrance slit of the spectrometer, and fibre optic array were all enclosed in black cardboard boxes so that no light could reach the photomultipliers except through the field stop aperture. The entrance slit of the spectrometer was also masked so that only the image of the discharge passed through the slit and all else was blocked. It was found that a significant amount of light was reflected off the front window, scattered

from the excimer body, and reflected back into the collection lens. So a small beam dump was placed beneath the excimer laser body to intercept this light.

The size of the expected Thomson scattered signal can easily be calculated. By intuition we can write

$$\frac{P_s}{P_i} = r_0^2 n_e L d\Omega \qquad ...(3.1)$$

where L is the scattering volume length. Assuming that the collection lens has an aperture of 24 mm diameter and is 2.3 m from the centre of the excimer laser, equation (3.1) gives a ratio of scattered power to incident power of 8.6×10^{-15}. Assuming that the incident energy is 40 mJ, this means that the collection lens will receive 92×10^3 photons - sufficient for this experiment.

3.5 Optical System Alignment

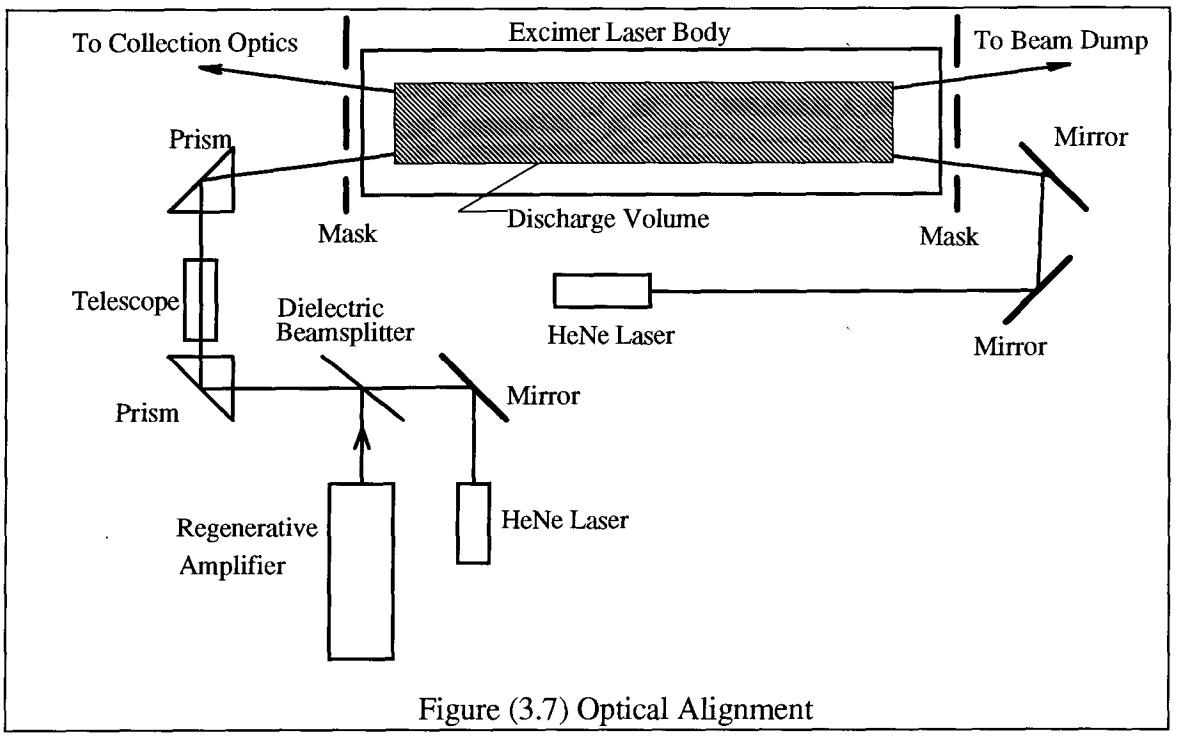

Figure (3.7) Optical Alignment

Careful alignment of the probe beam and collection lens was done to ensure that the entire discharge volume was in the field of view of the collection lens and that the

scattering angle was as desired. Most of the alignment was done with the use of two metal masks. Each consisted of a piece of aluminum with a pair of 2 mm pinholes drilled with their centres separated by 8 mm. These were placed just outside of the excimer windows (see figure (3.7)).

A HeNe laser beam was set up so that its beam would pass through a 532 nm dielectric mirror (transparent at the 632 nm HeNe laser wavelength) and follow the path of the injection pulse. This beam could therefore be used for alignment. Similarly, another HeNe laser beam was sent the other way through the discharge volume, the collection optics, the spectrometer, and to the imaging device as shown in the diagram.

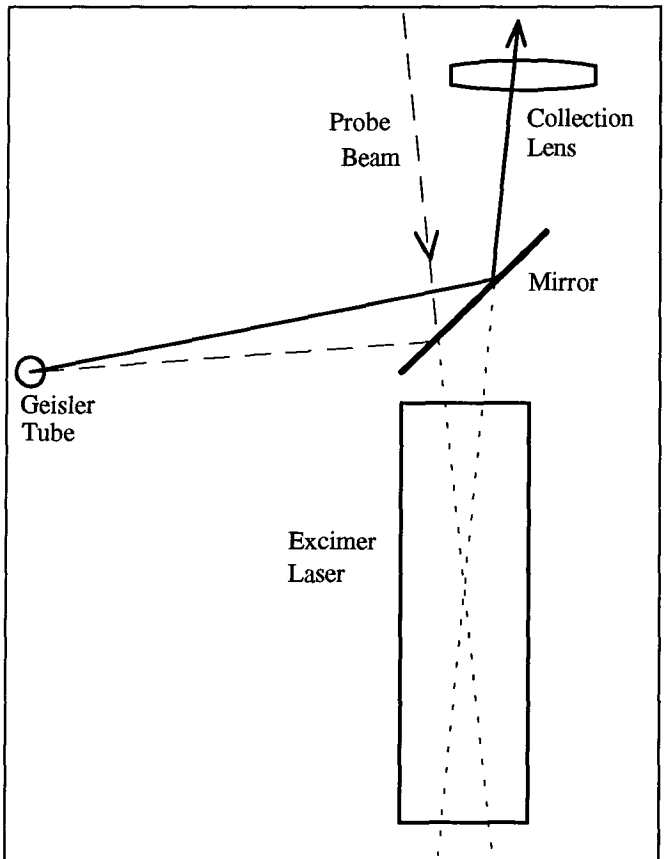

Figure (3.8) Collection Lens Focusing Arrangement

It was also necessary to focus the scattered light onto the entrance slit of the spectrometer with the collection lens. This was done by placing a mirror in front of the excimer laser and placing a He Geisler tube, oriented vertically, in the path of the probe beam, the same optical path length away from the collection lens as the centre of the excimer would be (see figure (3.8)). The image of the Geisler tube would be focused onto the closed slit of the spectrometer by changing the position of the lens.

3.6 Scattered Light Dispersion

As previously mentioned, a grating spectrometer was used to spectrally disperse the signal. The spectrometer was constructed in what is known as the Ebert arrangement shown in figure (3.9). The large collimating mirror shown has a radius of curvature of 25 cm.

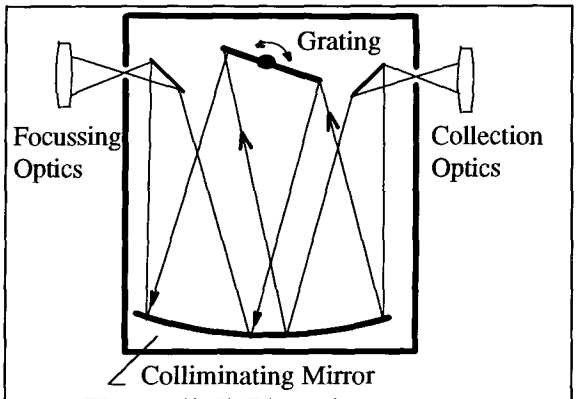

Figure (3.9) Ebert Arrangement Spectrometer

The grating had an area of 64 mm by 64 mm and had 1180 grooves/mm, the grooves being oriented parallel to the direction of polarization.

The intensity of a monochromatic signal reflected from a grating can be described as

$$I(\varphi_2) = D(\theta_1, \varphi_2, \lambda) \left| \frac{\sin\left(\frac{\pi M p}{\lambda}\right)}{M \sin\left(\frac{\pi p}{\lambda}\right)} \right|$$

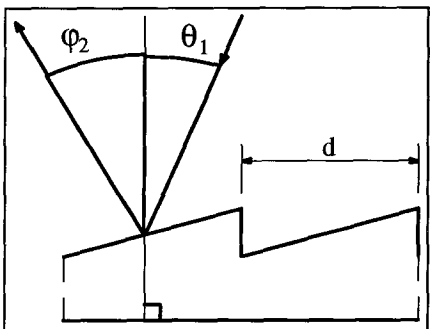

Figure (3.10) Grating Definitions

where M is the total number of rulings and $p = d(\sin\theta_1 - \sin\varphi_2)$ is the path difference between parallel rays reflecting off adjacent rulings and $D(\theta_1, \varphi_2, \lambda)$ is the diffraction pattern of an individual facet. θ_1, φ_2, and d are defined in figure (3.10) The facets of the grating are cut at an angle to the plane of the grating so that at a specified wavelength the angle of reflection is the same as the angle of maximum diffracted intensity. This particular wavelength is known as the blaze wavelength. The grating used was blazed for 600 nm. For a spectrometer, the resolution can be defined as the smallest wavelength difference, $\Delta\lambda$,

such that when two monochromatic lines, differing by $\Delta\lambda$ are input into the spectrometer, the widths of the diffracted lines are equal to the separation of their central maxima.

It can be seen that as the number of grooves increases, the resolution will also increase. For high resolution, the light incident on the grating must be highly collimated. Therefore, to optimize the resolution of the spectrometer, two things can be done:

1. The f number of the signal can be matched to the f number of the spectrometer so that the entire grating is covered;
2. The entrance slit of the spectrometer can be narrowed down until the width of the transmitted signal is diffraction limited.

Unfortunately, for most of these experiments, the full grating was not illuminated. In order to minimize stray light entering the spectrometer, the field stop aperture was employed to keep the f number of the collection lens large (f/12.8). This meant that the resolution obtainable was 3.5 times less than that theoretically possible: the grating could theoretically resolve lines 0.2 nm apart instead of lines 0.06 nm apart.

The slit width used for most of these experiments was determined to be 320 μm. Given a collimating mirror focal length of 25 cm, the width of this entrance slit would create an uncertainty in the incident angle, θ_1, of 1.3×10^{-3} rad which created an uncertainty in the diffracted angle, φ_2, of 9×10^{-4} rad. The loss of resolution from the finite width of the entrance slit was calculated to be much smaller than the loss of resolution due to the finite number of rulings.

3.7 Streak Camera

A streak camera is a device which allows the high temporal resolution of a one dimensional spatial image. Light passing through a horizontal slit is imaged onto a

photocathode converting an optical image into an electron image. This image is accelerated and passed between parallel deflection plates as shown in figure (3.11). A sweep voltage is applied to these plates at an appropriate moment so that electrons arriving at different times will have different vertical displacements on the phosphor screen and the horizontal image will remain unaffected. The phosphor image is

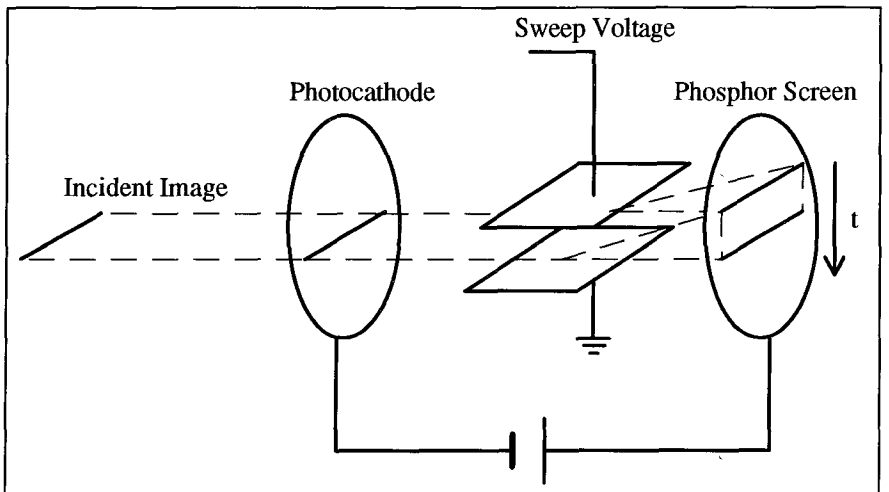

Figure (3.11) Principle of Streak Camera Operation

recorded by a video camera.

The streak camera used was a Hammamatsu 979 Temporal Disperser attached to a C1000 video camera and a C1440 Frame Memory Image Analysis System. Five gain settings were available. The speed most commonly used scanned the full screen in 5.42 ns.

The lens combination used between the entrance slit of the streak camera and the streak tube was a 105 mm, 35 mm pair giving three times magnification. The streak camera entrance slit was either put directly against the output aperture of the spectrometer to collect a higher intensity signal with lower resolution or separated with a magnifying arrangement to provide better spectral resolution but lower intensity. Unfortunately, it was found that there was not enough dispersion to get useful results when the camera was placed directly against the spectrometer.

While a spherical lens magnification arrangement would have been preferable to a cylindrical one due to the simplicity of alignment one was found to be inadequate due to the light lost at the streak camera entrance slit due to the magnification in the

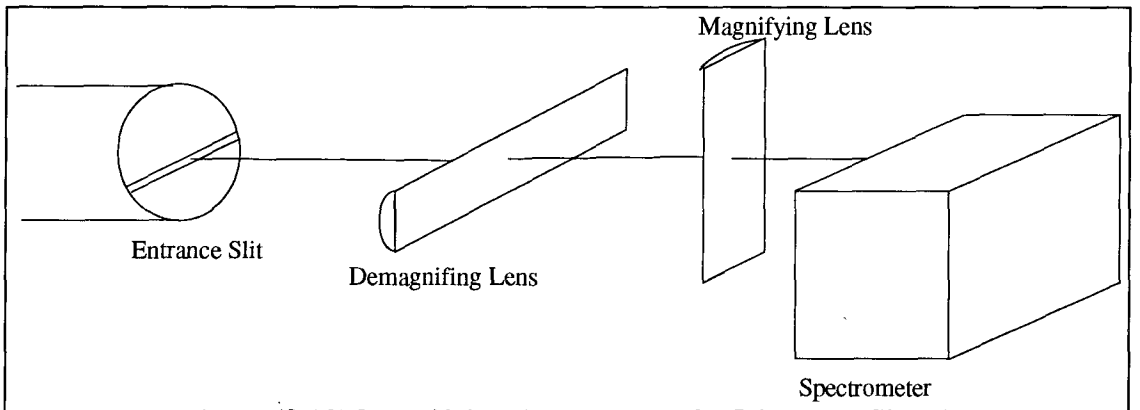

Figure (3.12) Magnifying Arrangement for Dispersed Signal

vertical direction.

Using cylindrical lenses arrangement, as shown in figure (3.12), it was possible to have a reasonable magnification in the horizontal plane while focusing all the light in the vertical direction onto the horizontal entrance slit of the streak camera. The lenses used each had a focal length of 7 cm, a width of 5.5 cm, and a length of 22 cm. The streak camera was placed approximately 0.75 m from the spectrometer with the lenses placed at the appropriate positions to achieve the proper focus.

Two dimensional angular adjustments had to be made to all components since there was an internal misalignment in the spectrometer. This meant that the output signal was not traveling parallel to the table and the direction of dispersion was not horizontal. These problems introduced distortion into the signal. It was discovered that the streak images obtained did not have a precisely vertical time axis and that as the streak camera grating was rotated, the intensity of the signal would vary. It was assumed that the variation wasn't significant on the wavelength scale of the dispersed image.

In order to reject light at 532.0 nm while accepting the spectrally dispersed Thomson scattered light, for some preliminary experiments, a very thin piece of black tape was placed vertically across the horizontal slit to block out the signal exactly at 532.0 nm. In this way, the full intensity of the dispersed image could be imaged on the streak tube with maximum gain without damaging the system. However, it was found that when all sources of stray light were successfully eliminated, the total signal was not bright enough to damage the camera so the mask was removed.

Alignment, focusing, and calibration of the streak camera was done with a highly attenuated HeNe laser passing through the excimer laser, collection optics, and spectrometer as described in section (3.5). Further focusing was done by focusing the spectrally dispersed image of a He Geisler tube onto the streak tube and watching the image on the video display. The Geisler tube was positioned as shown in figure (3.8).

With this experimental arrangement, the best time resolution attainable is approximately 2.5 ns due to differing delay times introduced by the scattering volume length. In practice, the time resolution would be a bit lower due to the width of the streak camera entrance slit needed to get an appropriate intensity on the streak tube. The streak images were transferred to a personal computer and analysed. The analysis program was written by Y. Zhu with modifications by myself.

3.8 Photomultipliers

The three photomultipliers used were RCA 8575's operated with a -1700 V bias. It was found that the photomultipliers had to be operated inside the screened room to avoid the pickup of noise created by the spark gaps. To get good coupling between the fibres and the photomultiplier tubes, the bundles were epoxied into a hole drilled in a brass plug. The plug and the fibres were then polished. The plug was then fitted into a jacket so that the fibre abutted a Plexiglas window. The photomultipliers were

mounted in such a way as to abut the window from the other side as shown in figure (3.13). The image from the spectrometer was magnified nine times and imaged onto the fibre optic array. The physical size of each fibre optic channel was 1.6 mm wide and 2.5 mm high. Due to the height of these channels and the use of the spherical lens for magnification, the alignment problems experienced with the cylindrical lenses and the streak camera were not experienced with this arrangement.

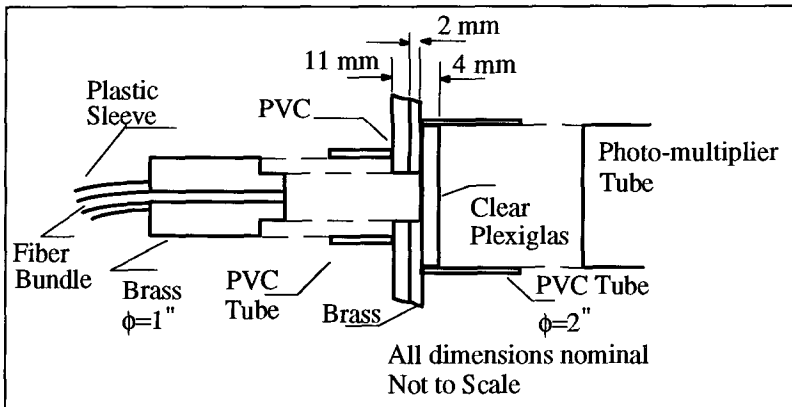

Figure (3.13) Photomultiplier Tube Coupling with Fibre Optic Bundle

To reduce electronic noise, the photomultiplier tubes were wrapped in copper sheaths which were kept at the cathode potential and all the tubes were enclosed in a larger copper sheath kept at ground potential.

The photomultipliers were calibrated by measuring the voltage signals from the probe light reflected off a white card placed at the same optical path length as the excimer see figure (3.14). It was assumed that the light reflected off the card was essentially monochromatic. Voltage signals were taken as a function of the wavelength reading on the spectrometer. Care was taken to always turn the spectrometer dial in only one direction to avoid backlash. The results are shown in figure (3.15). Using this information, the wavelength separation between channels was found to be 0.6 nm. A better calibration was not performed because ultimately the calibration was not needed.

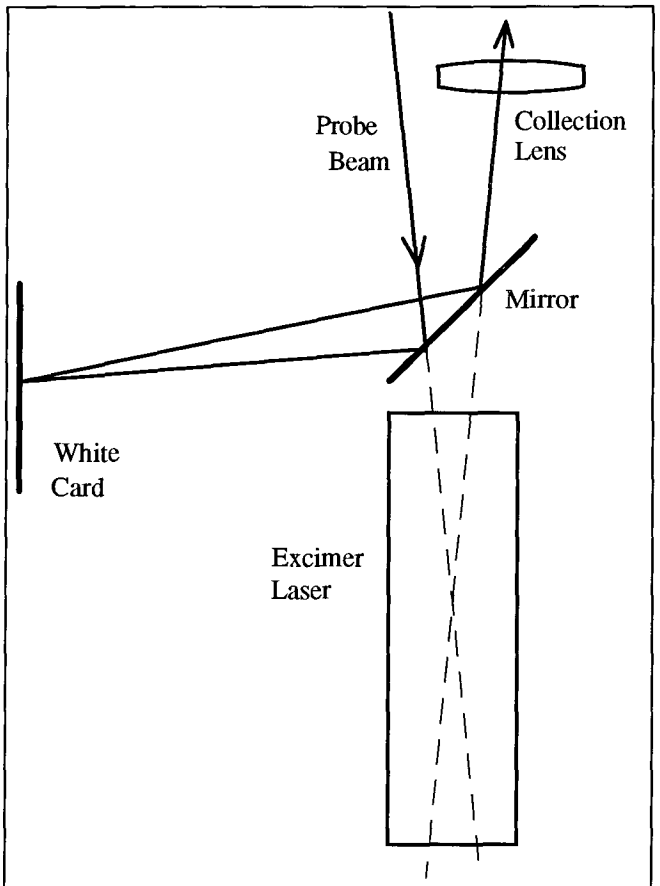

Figure (3.14) Photomultiplier Tube Spectral Dispersion Calibration Arrangement

Unfortunately, with the photomultipliers, the best time resolution attainable was about 5 ns. This was not good enough to distinguish the noise from the end windows from the signal as it was possible with the streak camera. The streak camera images showed that the intensity of the reflected signal from the end windows would be sufficiently large to hide any Thomson scattered signal as will be shown in chapter 5. The temporal resolution was estimated

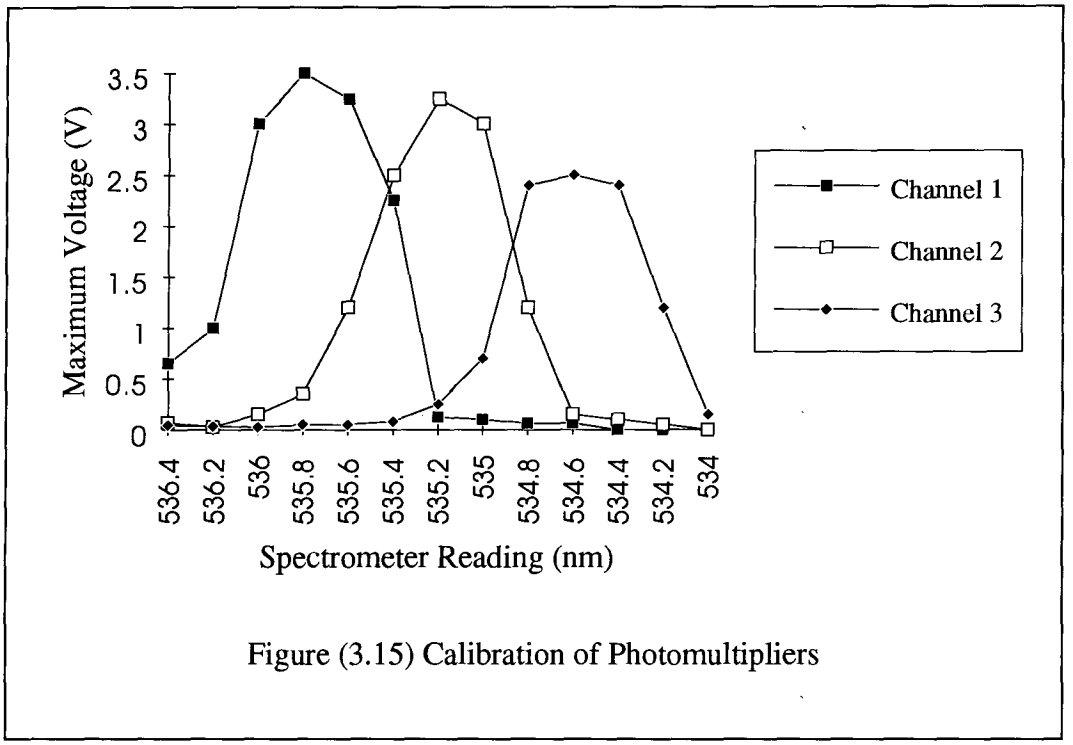

Figure (3.15) Calibration of Photomultipliers

to be the full width at half maximum of the signal from a single electron emitted by the photo-cathode which was on the order of 5 ns (see figure (3.16)).

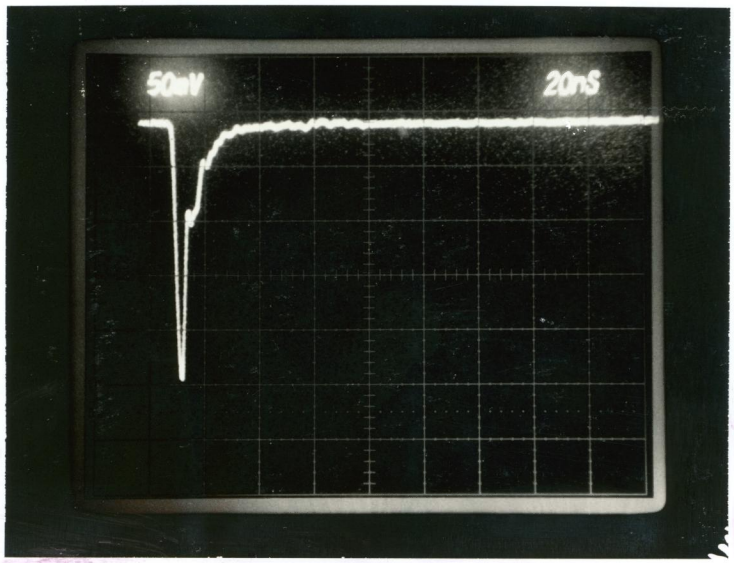

Figure (3.16): Photomultiplier Voltage for a Single Photon.

3.9 Electronic Measurements

Special precautions had to be taken to counter the high level of radio frequency noise created by the sparkgaps and the excimer discharge which affected electronic measurements and created false timing signals. The two Tektronics oscilloscopes were housed in a screened room to avoid electrical interference. This room is constructed with double walls of fine copper sheet connected to the ground potential at only one point. The power lines were passed through a noise filter and the coaxial signal cable shields were grounded at the wall. An electronic schematic diagram of the measurement apparatus is shown in figure (3.16).

The photomultipliers were particularly sensitive to noise. As a result they had to be housed within the screened room. As previously described, the output from the spectrometer was magnified onto an array of fibre optic bundles. The fibres were then passed through a small hole in the walls of the screened room and coupled to the photomultipliers.

To perform this experiment, it was necessary to measure the photomultiplier voltage signals, the current through the plasma, and a photodiode signal of the injection pulse. Unfortunately, when the excimer laser was fired, the photodiode signal was overwhelmed by the radio frequency noise created by the discharge. Arrangements could have been made to remove most of this noise but, due to the lack of positive results, it was not felt that this would be productive.

The excimer discharge current was measured with a linear Rogowski coil. This

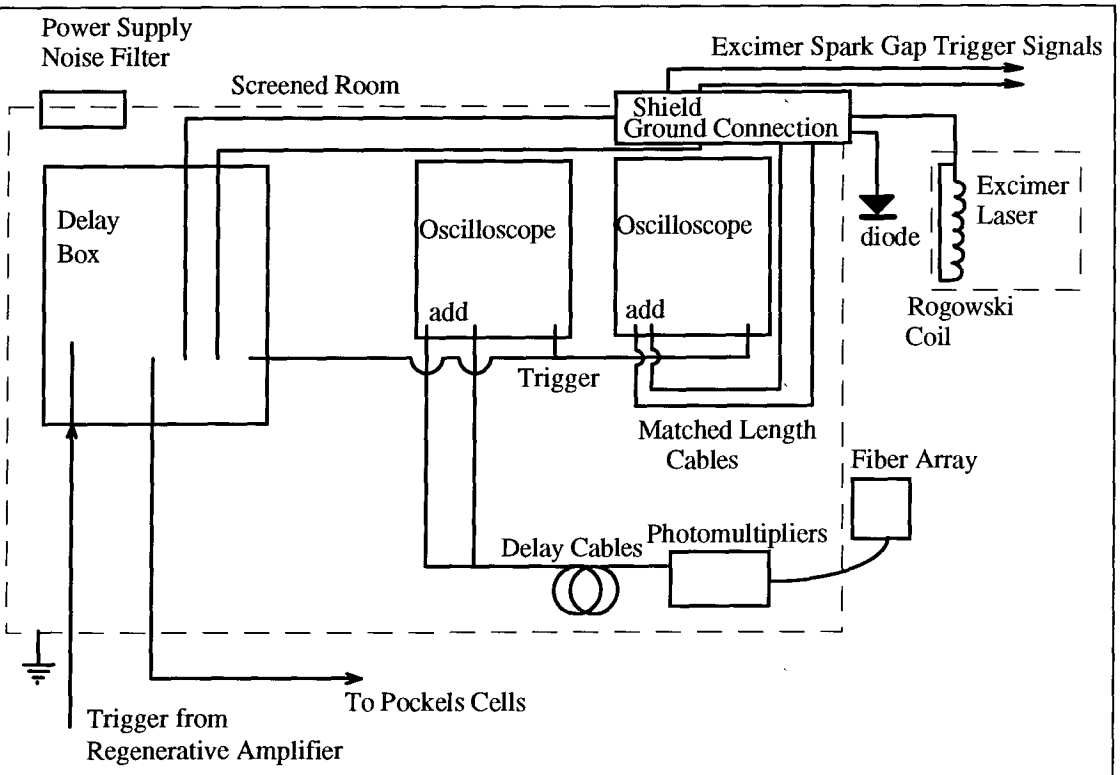

Figure (3.17) Measurement Apparatus

coil simply consisted of a copper wire wrapped around an insulator N times. When the

current passing through the plasma produced a changing magnetic field, the changing flux through the coil induced a proportional voltage in the coil as predicted by Ampere's law.

The Rogowski coil was placed alongside the excimer body and under a row of capacitors so that the current flowing through the upper electrode could be directly monitored. A sample of the Rogowski coil voltage is shown in figure (3.18).

The photodiode was placed so as to pick up light reflected from one of the lenses of the telescope.

Since we had only two oscilloscopes, we had to delay the signals from the two of the three photomultipliers and add them together at the inputs. One signal was delayed by 100 ns and another by 700 ns.

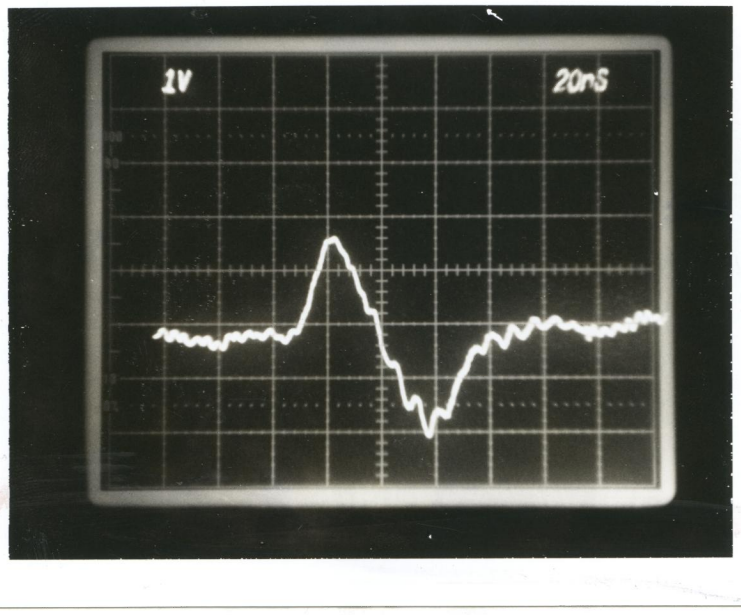

Figure (3.18) Rogowski Coil Current as Seen on Oscilloscope

4 Electronic Timing and Synchronization

The timing of all the components is crucial to the success of this experiment due to the short injection pulse duration (≈ 100 ps) and the low repetition rate (≈ 0.02 Hz). The injection pulse must coincide with the excimer laser discharge and the measurement apparatus must be triggered at appropriate times in order to capture the signal.

This chapter will be organized into sections describing first how the components of the regenerative amplifier are timed to each other then how the excimer laser and the measurement apparatus are timed in relation to the regenerative amplifier.

A non-commercial electronic delay box was used as the primary delay device. The delay could be varied from 0.0 to 999.9 μs in steps of 0.1 μs. The delay box was triggered from the differentiated pulse from the flashlamp trigger pulse; the Pockels cells and excimer laser trigger pulses were produced at appropriate times later.

4.1 Regenerative Amplifier

In the previous chapter, a simplified explanation of the operation of the regenerative amplifier was given. In this chapter the electronic subsystems will be described. These can be considered as comprising of three subsystems, the Control Unit, the Power and Capacitor Bank Units, and the Laser Bench Unit. Each subsystem will be described in turn.

The effect of the controls to be described was to keep the jitter in the timing of the green pulse as seen on the oscilloscope below approximately 3 ns. However, this could have been caused by jitter in the delay box or in the oscilloscope triggering circuit and was not necessarily entirely due to the RGA.

4.1.1 Control Unit

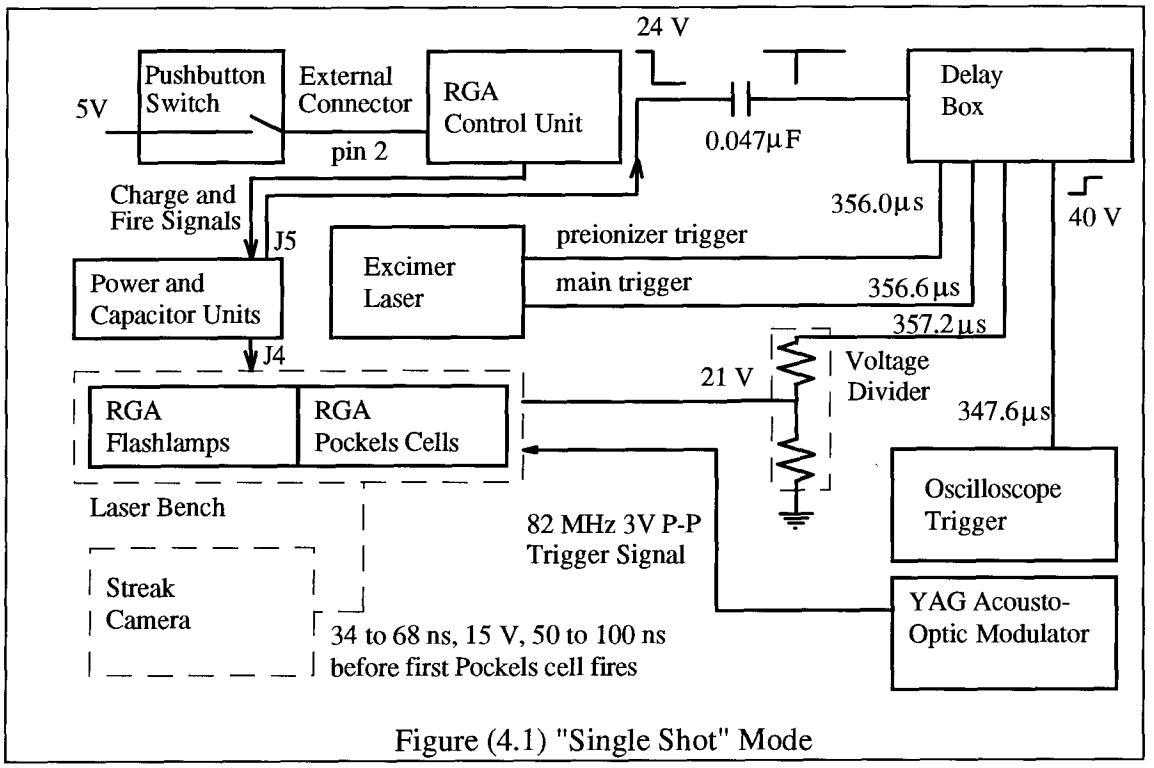

Figure (4.1) "Single Shot" Mode

At the heart of the regenerative amplifier is the Control Unit. As the name implies, the Control Unit controls the operation of the Power Units and Capacitor Banks. It sends charge signals to the flashlamp Power Unit and sends a fire signal to the flashlamps as soon as the capacitors are charged. These signals are sent at a predetermined rate between 5 and 10 Hz, triggered manually through two pushbuttons on the control panel, or triggered externally though the "external connector". For this experiment, either the flashlamps were fired repetitively and automatically ("fixed" mode) or controlled externally ("single shot" mode). Diagrams of each mode are shown in figures (4.1) and (4.2). These diagrams will be gradually explained throughout this chapter.

The first mode, dubbed the "single shot" mode, utilizes the external triggering circuitry of the regenerative amplifier Control Unit. The interface is a 9 pin external connector. Table (4.1) lists all the connections made. As can be seen, pin 2 is the only one used dynamically; a pushbutton switch is used to connect the high voltage from the power supply to the pin when a shot is

desired. The other pins are fixed either at 0 or 5 V. Pin 3 could be used to fire the flashlamps but is set so that they are fired as soon as an end of charge signal is received.

The "fixed" mode was used to produce a maximum single shot power. In this mode, an internal clock sent charge signals to the Power Unit at a fixed rate between 5 and 10 Hz. As soon as a end of charge signal was received from the Power Unit, a trigger signal was sent from the Control Unit to the Power Unit to fire the flashlamps (see figure (4.2)).

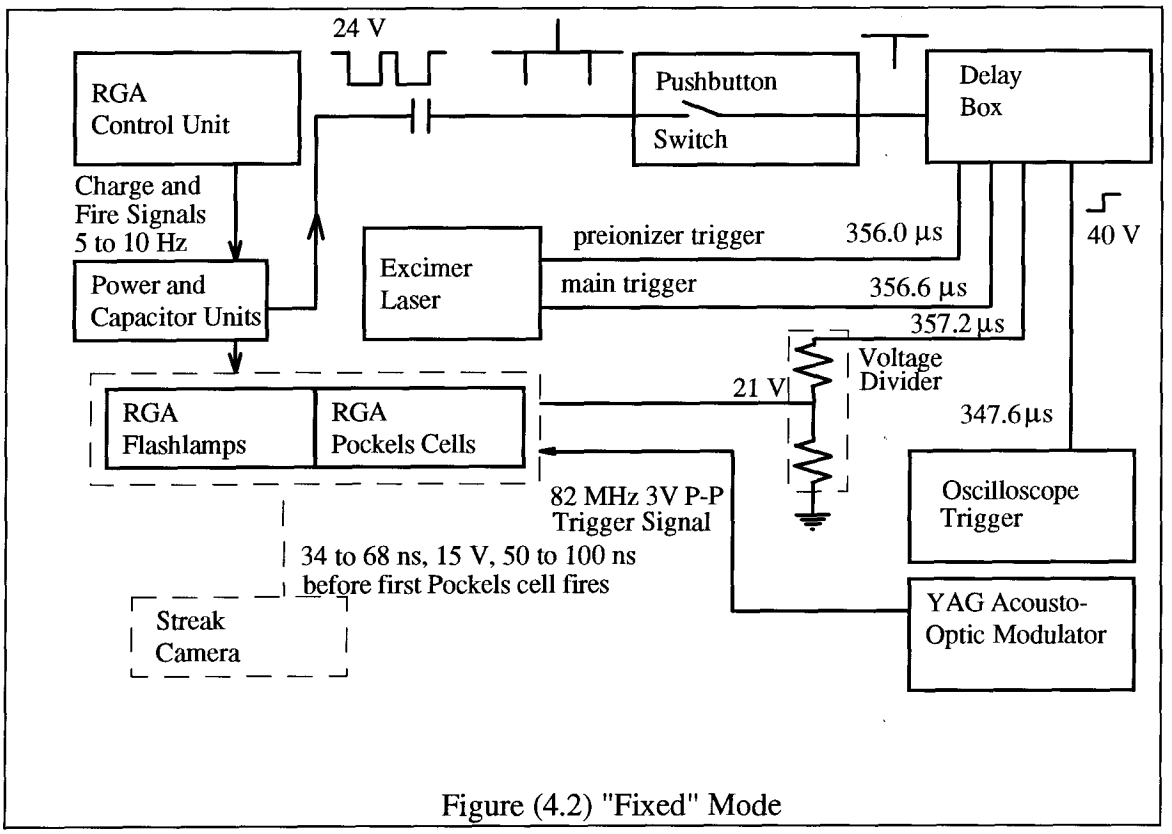

Figure (4.2) "Fixed" Mode

Pin 1: Power supply ground
Pin 2: Charge command 0 to 5 V
Pin 3: 5V. Fire command
Pin 4: 5V. needed to provide an end of charge signal
Pins 5 through 9: not used.

Table (4.1) External Connector Pin Assignments for "Single Shot" Mode

4.1.2 Power and Capacitor Banks

The regenerative amplifier needs two sets of Power Units and Capacitor Banks: one for each laser rod. As mentioned before, the Control Unit sends identical charge and fire signals to the Power Units. As soon as the charge signals are received, the Capacitor Banks are charged to the pre-selected voltage of close to -1700 V. This voltage can be adjusted by a dial on the front panel of the Power Unit. Slight adjustments are occasionally needed to maximize the output power. Once the capacitors are charged, the end of charge signals are sent to the Control Unit.

When the fire signals are received, fast -17 kV ionizing pulses are sent to the flashlamps followed by the flashlamp voltage pulse which has a duration of 180 μs (FWHM). At the same time, a 24 V high to low signal is sent from the resonator Power Unit to the external electronics via a BNC output, denoted J5, which fires the Pockels cells after an appropriate delay. The 24 V signals were differentiated by a 0.047 μF capacitor. This differentiated signal could be used to trigger the delay box.

4.1.3 Laser Bench Controls

The frequency scaler unit controls the timing of the Pockels cells in relation to an external signal and the seed mode locked pulse train. This unit takes the 82 MHz signal from the oscillator

acousto-optic modulator and converts it to a fast TTL signal for its own use. When the appropriate trigger signal is received from the external electronics a switch is set so that the first Pockels cell is fired at the beginning of the next cycle and a 15V trigger signal is sent to a BNC port marked "sync out". At the same time a delay line is activated so that after an appropriate number of clock cycles, the second Pockels cell is supplied with the quarter wave voltage to switch the amplified pulse out of the oscillator.

The input radio frequency synchronization signal from the YAG acousto-optic modulator had to have a peak to peak voltage of 3 V and the trigger signal from the delay box had to have a nominal voltage of 15 V. A voltage divider was used to attenuate the 40 V delay box signal.

Occasionally adjustments had to be made to the relative timing of the first Pockels cell to the second one in order to get the maximum possible power out.

4.2 Delay Box

The 24 V signal from the J5 output of the Power Unit was differentiated by a 0.047 μF capacitor. This differentiated signal could be used to trigger the delay box. In the "single shot" mode the signal goes directly to the delay box as shown in figure (4.1). In the "fixed" mode, a pushbutton switch is used to connect the trigger signal to the delay box when desired: as shown in figure (4.2).

The 16 channel delay box was used to provide 40 V positive edge trigger signals to the rest of the system. Signals from the delay box triggered the Pockels cells at the appropriate times as well as fired the excimer preionizer and excimer main discharges. It also provided the appropriate trigger signals for the oscilloscope. The delays used are indicated on figures (4.1) and (4.2).

4.3 Streak Camera

The streak camera was triggered by the 15 V low to high "sync out" signal from the regenerative amplifier 50 to 100 ns before the first Pockels cell was fired. It was triggered with

this synchronization signal instead of with a photo-diode because the delay between the input trigger pulse and the streak camera operation was at least 28 ns. This would imply an unreasonable optical path delay. Adjustments to the timing of the streak camera in relation to the scattered signal was done by manipulation of a 0 to 32 ns delay box with increments of 0.25 ns supplemented by appropriate delay cables. To time the injection pulse and the streak camera properly, small targets were set up at the entrance and exit windows of the excimer; the reflected signals from which could be seen very clearly on the streak camera. Thus appropriate delay adjustments could easily be made.

4.4 Measurement Apparatus

In order to see the measured signals at the appropriate times, a fourth channel of the delay box was used to trigger both oscilloscopes at the same time. The BNC co-axial cables from the photodiode and the Rogowski coil were made the same length so that accurate time comparisons could be made. The diode was operated with a 27 V bias.

5 Measurements and Results

In this chapter, the measurements taken by the streak camera and the photomultiplier tubes and how they were analysed is discussed. This is followed by a section discussing all the results as a whole.

5.1 Streak Camera

At first, measurements were made with the streak camera. A representative example of a streak camera image is shown in figure (5.2). The density of shading is proportional to the intensity of the signal. Indicated are the time and wavelength axes. The signal can be seen in the middle between the scattered signals from the two end windows. The data were recorded as a 512 by 512 pixel matrix with each pixel having an intensity value between 0 and 255.

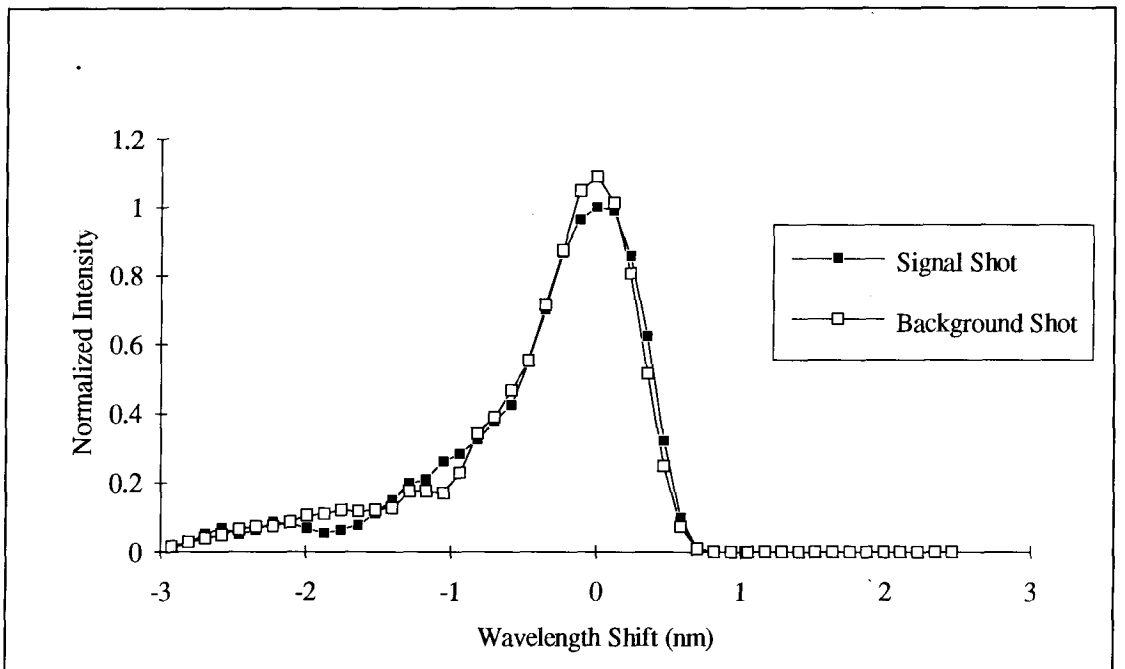

Figure (5.1) Wavelength Spectrum of Scattered Light

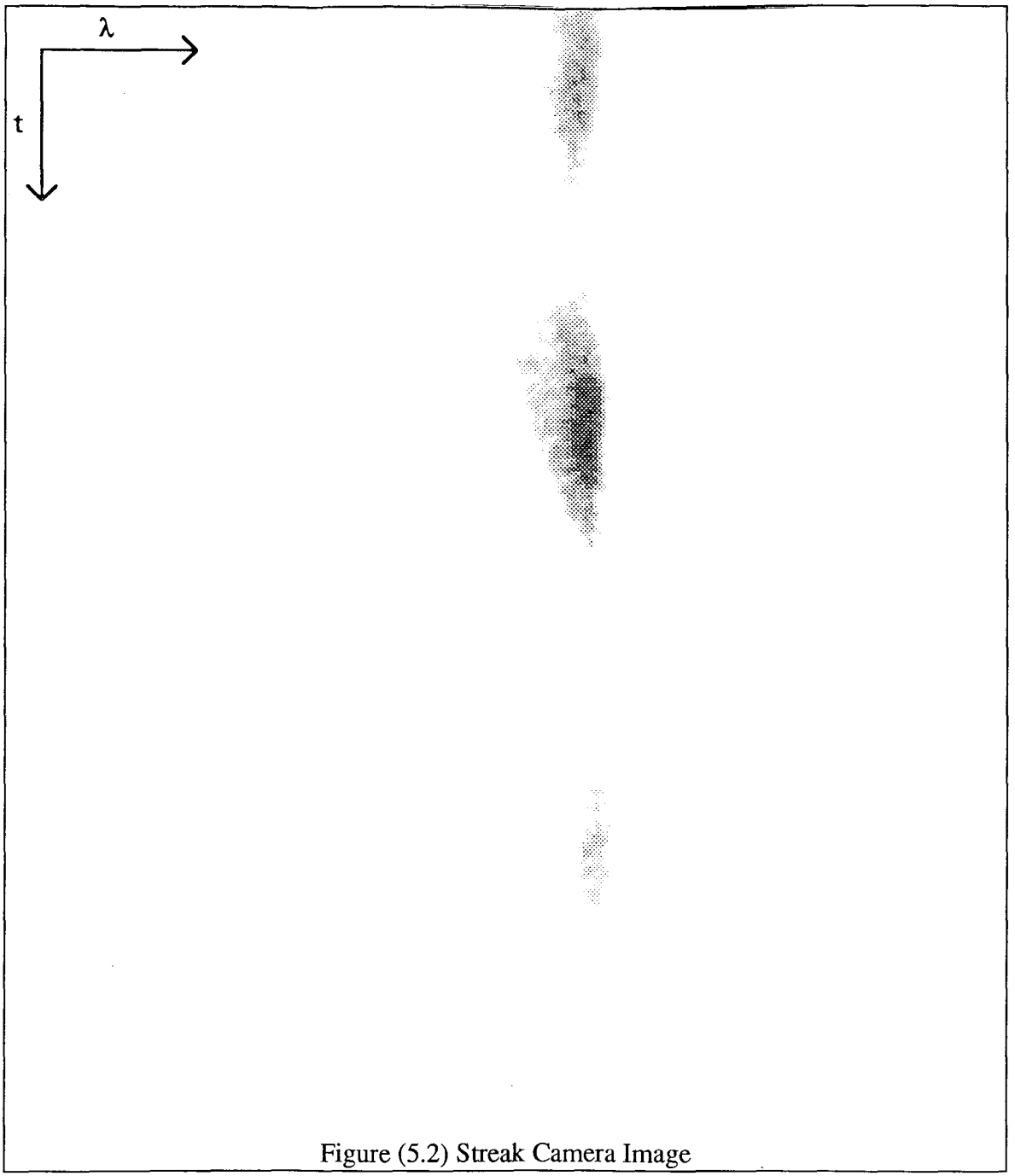

Figure (5.2) Streak Camera Image

The position of the Rogowski coil current in relation to the probe pulse on the oscilloscope screen was recorded for each streak record so that the recorded scattered signal could be related in time to the excimer pulse. Similar data were also recorded for cases when the probe beam was fired without an excimer discharge. These data could be used as a background level.

To analyse the raw data, the signal and background shots were compared. Figure (5.1) shows the data in figure (5.3) temporally averaged over 0.75 ns around the maximum intensity. Also shown is a similarly treated background signal.

Since the intensity of the probe beam would have been slightly different for each shot, in analysis, the puls powers were all normalized to equal values. It is valid to simply scale the signals since the scattered intensity for any effects that we have considered is proportional to the incident intensity. From figure (5.1), it can be seen that there is no significant difference between the two shots. Therefore any Thomson scattered signal is much smaller than the noise signal.

Assuming an electron temperature of approximately 2 eV[1], the full width half maximum of the signal should have been approximately 3 nm. In figure (5.1), the spectrum has a Full Width at Half Maximum (FWHM) of approximately 0.8 nm. Any signal that we would be able to detect therefore would be the portion shifted by more than approximately 0.5 nm. Since we could not find any signal at such shifted wavelengths and since this streak record was taken with maximum gain and maximum practical streak width, it was decided that the much more sensitive photomultiplier tubes would have to be used. The photomultiplier tubes had the additional advantage of being easily able to reject the noise signal at 532.0 nm simply by tuning the spectrometer.

The streak camera results were very useful in determining where the excess stray light was coming from as deduced from the timing information produced. From these results it was determined that the majority of stray light was coming from the front and back windows. In fact, over half the intensity reaching the streak camera was scattered light from the windows. This could easily be seen in figure (5.3) which was made by taking the signal from figure (5.1) and integrating it over the wavelength axis to find the intensity reaching the camera at any particular time.

Since the Rayleigh scattering cross section in relation to the Thomson scattering cross section is well known for helium, an estimate of the noise expected can easily be made. DeSilva and Goldenbaum[29] give $\sigma_T/\sigma_R=2750$ which leads to an estimate of the ratio of the scattered intensity to the incident intensity of 1.4×10^{-7} which is eight orders of magnitude above the Thomson scattered signal.

Rayleigh scattering was probably the cause of much of the noise seen. Rayleigh scattered light originates from oscillating atomic dipoles excited by the incident radiation. Any wavelength shift arises from the motion of atoms in much the same way as the wavelength shift occurs in Thomson scattering; however, at room temperature, the Rayleigh scattered signal is essentially monochromatic for monochromatic probe light.

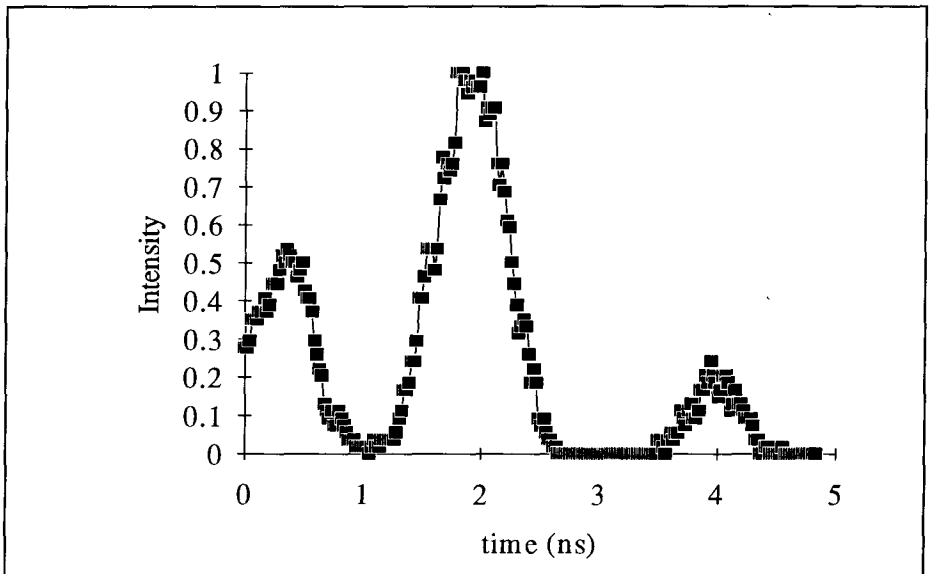

Figure (5.3) Analysed Streak Camera Image

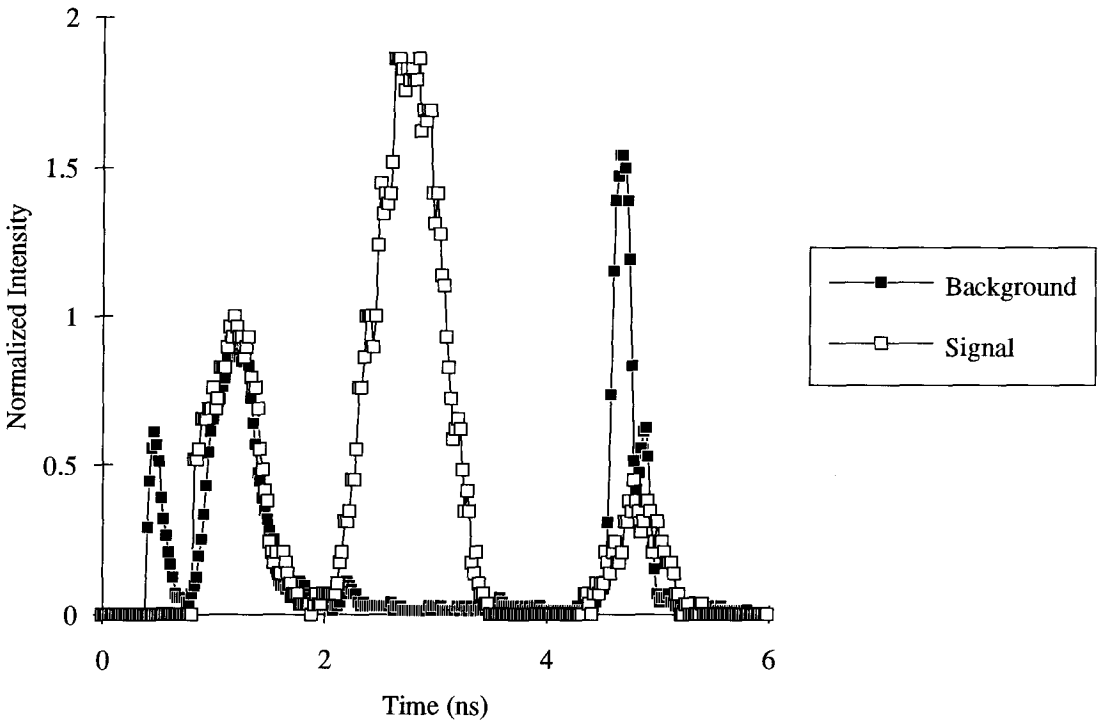

Figure (5.4) Background and Signal Time Signals to show Rayleigh Scattering

This was definitely shown in the experimental results. There was a great difference in noise signals between when the excimer body was filled with gas and when it was evacuated. Figure (5.4) depicts the signal shot shown previously compared to a background shot taken when there was no gas in the excimer laser body. To obtain this figure, first the two images were time shifted so the front window reflection peaks coincided then these peaks were normalized to the same value.

5.2 Photomultiplier Tubes

A typical voltage signal from the photomultiplier tubes, as seen on the oscilloscope, is shown in figure (5.5) for when the excimer is firing, and in figure (5.6) for when it is not.

In general, in order to see if any signal could be distinguished from the noise, ratios between these voltages were taken and compared statistically. It was necessary to use ratios instead of the absolute voltages as, when the excimer was firing, the probe pulse power could not be measured with the present arrangement. There were no significant differences found for any of the data sets: each consisting of 20 to 40 shots. Attempts were made using the laser gas mixture as well as pure helium at pressures of 3.7 atm and

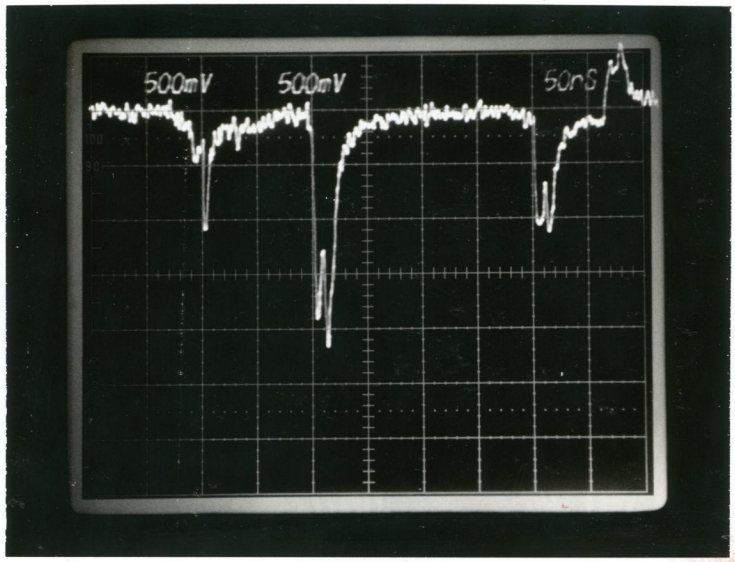

Figure (5.5) Typical Photomultiplier Tube Signals with an Excimer Discharge

5.3 atm. There were no significant differences found between these cases either. However, there were large differences when there was no gas in the excimer compared to when there was gas, again confirming the suspicion that the majority of the noise was from Rayleigh scattering.

Along with the photomultiplier data with each shot, measurements were made of the differentiated excimer current when the laser was firing and the diode voltage when it was not. It should be noted that the excimer current traces within each data set were identical within the experimental uncertainty (recall that the diode signal was not usable when the excimer was firing).

5.3 Discussion

There were a few problems with the experiment that made measurement of the electron velocity distribution impossible: poor resolution, large noise signals at the laser frequency, and possibly laser induced heating.

5.3.1 Resolution

All of our results were affected by a lack of resolution. In order to determine

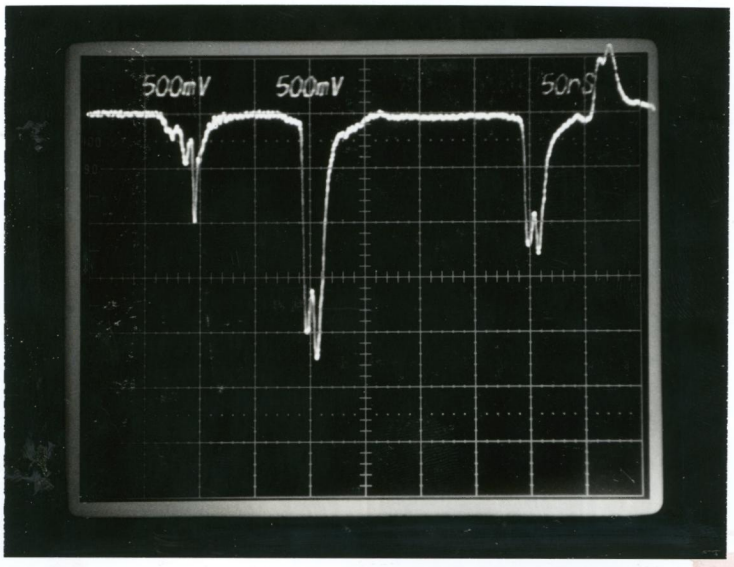

Figure (5.6) Typical Photomultiplier Tube Signals Without an Excimer Discharge

something about the resolution of the system, we can look at the measured widths of what should be essentially monochromatic signals: the Rayleigh scattered signal from the excimer gas and the scattered signals from the front and back excimer windows. Such signals are shown in figure (5.6) along with a signal that should show a Thomson scattered component. From the spectral width of the signals reflected off the front and back windows the resolution problems are readily apparent. The signals which are supposed to be essentially monochromatic - all except the one marked "signal" - have approximately the same widths as the signal shot. Furthermore, while the signal should be symmetric, there is a large "tail" on the negative wavelength shifted side of the spectrum.

Following is a list of a few possible explanations for the lack of resolution: only a small area of the grating was illuminated, the spectrometer entrance slit was opened too widely, scattered light from grating and magnification system was picked up by the measurement apparatus, or the dispersion system was slightly out of focus. Each probably contributes significantly to the total problem.

As mentioned in section (3.6), to mask out stray light, the field stop aperture in front of the collection lens was closed down to 24 mm. This meant that the f number (ratio of focal length to aperture diameter) of the collection lens was much greater than that of the spectrometer and therefore that the area of the grating used was much smaller than the total area. The reduction in the number of rulings used led to a theoretical resolution reduced by 3.5 times from the maximum possible resolution. This meant that the minimum theoretical resolvable wavelength difference would be approximately 0.1 nm. From figure (5.6) it is obvious that the resolution is much worse that this.

The second problem resulted from the fact that in an effort to collect the maximum scattered signal possible, the entrance slit to the spectrometer may have been opened too widely. However, from analysis, it can be shown that this wasn't the case. From the calibration data in figure (3.12), it can be seen that the FWHM of the photomultiplier channels was only 0.5 to 0.7 nm and from figure (5.1) it is 0.8 nm. Based on an entrance

slit width of 320 μm, the theoretical FWHM of a monochromatic signal would be less than

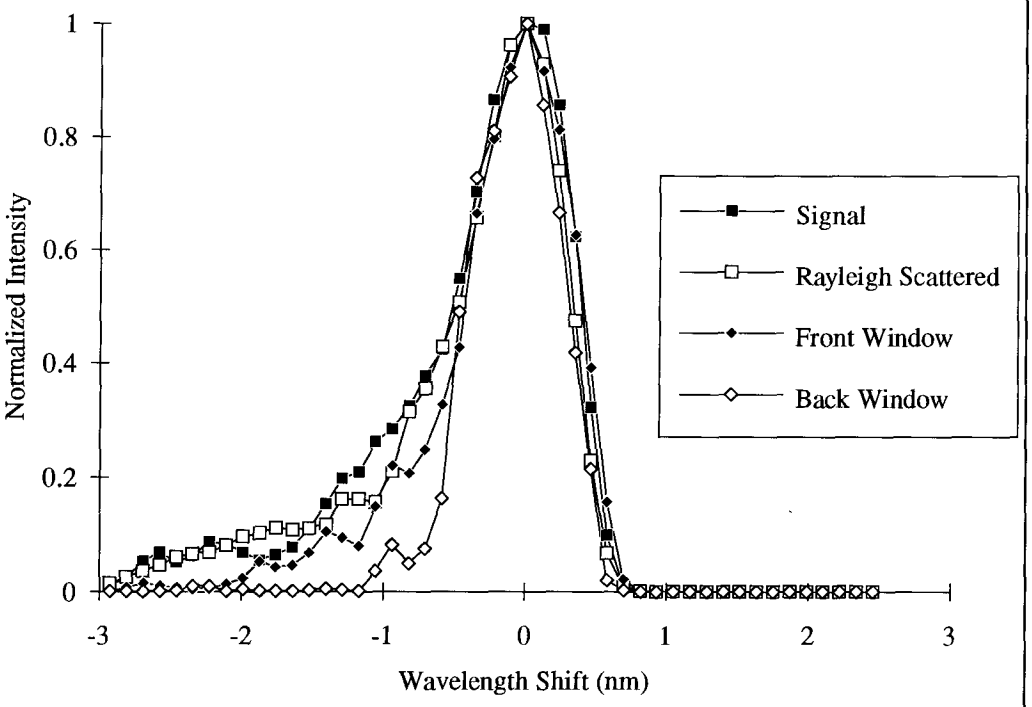

Figure (5.6) Signals Showing Resolution Problems

0.01 nm so the large entrance slit width does not cause a resolution problem.

Thirdly, there could have been a significant amount of scattered light from the grating and optics of the dispersion system. Again, this was not seen to be a major problem because the calibration measurements seemed reasonably good although not near what was theoretically possible.

Lastly, the focusing elements of the system could have been slightly mispositioned leading to less than optimal spectral resolution. However, this should have not been a problem at all because all of the optics were re-focused on a regular basis.

5.3.2 Noise

The second major problem was excessive stray scattered light at the laser frequency. It was this large amount of noise in relation to the Thomson scattered signal that made the lack of resolution such a problem. If the resolution was better, the stray light could simply have been excluded by masking it out.

The noise was scattered from a few sources: from the windows, the excimer electrodes, the excimer gas through Rayleigh scattering, or from dust.[29] A lot of effort was put into alleviating these problems as has been previously discussed in the apparatus chapter; however, large Rayleigh scattering signals will always be present and therefore improvements will have to be made to the resolution of the system. Further ways of reducing the noise signal are discussed in the following chapter.

5.3.3 Laser Heating Effects

Laser induced heating or a laser induced plasma could have affected all the results. Regarding figure (5.3), while the signal should come evenly from the entire scattering volume, the signal is entirely produced from the front of the excimer body. A possible explanation for this is that there was a laser induced plasma at the front of the excimer body. The free electrons would have presented a large scattering cross-section for the injected beam. However, the potential for such a problem was recognized shortly after photomultiplier tube measurements were started and hopefully corrected for by expanding the beam. There was no visible evidence of such heating; it would be expected that the breakdown would have been visible when looking through the excimer gas through a 532 nm filter but it was not.

It could also be possible that there was another laser heating effect similar to the one noted by Uchino et al[3]. They reported that it was not possible for them to perform measurements on plasmas containing xenon due to unexplained laser heating effects. It

was not known if our experiment suffered from a similar problem. Again, possible solutions to this problem are discussed in the following chapter.

5.3.4 Conclusions

In conclusion, the major problem affecting this experiment was the lack of spectral resolution. If this problem had been solved, it is felt that it would have been possible to measure the electron velocity distribution.

In addition, the major problem affecting the photomultiplier tubes was that the time resolution was not good enough. The considerable noise from the end windows could easily mask any signal given the lack of resolution.

The main problem affecting the streak camera measurements was that the gain was not high enough to measure the Thomson scattered signal at the extremes of the shifted wavelength spectrum.

6 Future Work

If this experiment were to be attempted again, it would be worthwhile to change the experimental arrangement to mitigate some of the problems mentioned in the previous section.

The biggest improvement might come about if a different scattering geometry was used. From a general survey of the literature, it seems that most experiments of this type have been performed with a scattering angle closer to 90°. This would greatly reduce directly scattered stray light. Such a change would also increase the time resolution of the experiment due to the shorter scattering length and resulting smaller range in round trip times. In order to do this, modifications would have to be made to the excimer laser body such as inserting a window in the side.

In an attempt to reduce stray scattered light, it would be beneficial to see if scattered light from dust in the chamber contributed significantly to the total noise level. This could be done by investigating how the signal varies with pressure. Any signal from dust particles wouldn't vary proportionally with pressure but would decrease with increased settling time between shots. To minimize any signal from dust in the chamber, it would be necessary to wait a significant amount of time between shots for all dust to settle down.

In order to get a measurable electron temperature, the helium buffer gas should be replaced with neon[20,30]. This would result in a higher electron temperature so that the spectrum of the Thomson scattered signal would be shifted farther out of the range of the noise spectrum.

Prior to another similar experiment, it would be worthwhile to investigate why a mixture containing xenon would suffer from the laser heating effect reported by Uchino *et al.* It would be necessary to look at the absorption spectrum of xenon atomic states and molecules. To see if this experiment experienced such an effect, it would be necessary to

perform the same type of analysis they did: it should be seen if the scattered signal power is proportional to the probe laser power as is desired.

To improve the experiment so that results would be more accurate and easier to obtain, a number of steps should be undertaken.

Firstly, it would be necessary to measure the intensity of the probe beam with every shot. That means it would be necessary to either screen the noise from the excimer laser better or to put the diode inside the screened room.

To facilitate the rapid collection of data more photomultiplier tubes should be used. This would allow a sufficient number of data points to find an accurate distribution with every shot. Presently, the grating would have to be rotated periodically so that a number of data points sufficient to calculate the distribution could be found. This method has defects arising from the need to take many shots and average the data. The current fibre optic array could possibly accommodate up to seven photomultipliers; however, an increased spectral dispersion would be necessary.

Even more desirable would be to decrease losses in the optical path before the excimer laser. The additional power in the signal would allow the streak camera to be used instead of the photomultipliers. The streak camera has advantages over the photomultipliers in that noise from the front and back windows does not interfere with measurements because it is temporally separated from the signal and that measurements done with the streak camera are easy to analyse because of the continuous wavelength spectrum. To increase the probe power, all the prisms could be replaced with dielectric mirrors and the lenses and flats could be anti-reflection coated.

To address the resolution problems mentioned in the previous chapter, the current spectrometer used should be replaced with a larger one with more resolution. Alternatively, a second spectrometer should be placed behind the first to additionally reject any stray light. Hopefully this would also alleviate the problem shown in figure (5.6)

where the spectrum isn't symmetric around the centre. It was never determined why this was so but it must have had something to do with the alignment of the spectrometer.

It might also be of interest to calibrate the photomultipliers with an absolute intensity so that the electron temperature could be measured at the same time as the electron density. A common method for doing this is to calibrate against the Rayleigh scattered signal. As previously mentioned, the electron density is an important parameter for modeling excimer lasers.

With such improvements, a successful experiment could certainly be performed.

References

1. A.Y. Elezzabi, M.Sc. thesis, University of British Columbia (1989).

2. H. Yamakoshi, M. Kato, K. Uchino, T. Iwata, M. Masuda, K. Muraoka, M. Maeda, M. Akazaki; Jap. Journ. Appl. Phys. 28, L1589 (1989).

3. K. Uchino, Y. Kubo, K. Muraoka, T. Sakoda, H. Yamakoshi, M. Kato, A. Takahasi, M. Maeda; J. Appl. Phys. 70, 41 (1991).

4. P. Millonni and J. Eberly, *Lasers* (John Wiley & Sons, Toronto, 1988).

5. A. Yarriv, *Quantum Electronics* (John Wiley & Sons, Toronto, 1989).

6. H. Griem, *Plasma Spectroscopy* (McGraw-Hill, Toronto, 1964).

7. G. Fiocco and E. Thompson, Phys. Rev. Lett., Vol 10, 89 (1963).

8. E. Thompson and G. Fiocco, MIT Research Laboratory of Electronics Quarterly Progress Report No. 69, 74 (1963).

9. M. Krauss and F. Mies, *Excimer Lasers,* ed C. Rhodes (Springer-Verlag, Berlin, 1983).

10. J. Ewing and C. Brau, Phys. Rev., Vol A12, 129 (1975).

11. J. Velazco and D. Setser, Jour. Chem. Phys., Vol. 62, 1990, (1975).

12. S. Searles and G. Hart, Appl. Phys. Lett., Vol. 27, 243 (1975).

13. J. Ewing and C. Brau, Appl. Phys. Lett., Vol. 27, 350 (1975).

14. E. Ault, R. Bradford, and M. Bhaumik, Appl. Phys. Lett., Vol. 27, 413 (1975).

15. R. Burnham, N. Harris, and N. Djeu, Appl. Phys. Lett, Vol 28, 707 (1976).

16. C. Wang, Appl. Phys. Lett, Vol 29, 103 (1976).

17. R. Burnham, E. Powell, and N. Djeu, Appl. Phys. Lett, Vol 29, 30 (1976).

18. W. Sarjeant, A. Alcock, and K. Leopold, Appl. Phys. Lett., Vol. 30, 635 (1977).

19. J. Mangano and J. Jacob, Appl. Phys. Lett., Vol. 27, 495 (1975).

20. M. Maeda, A. Takahashi, T. Mizunami, and Y. Miyazoe, Jap. J. Appl. Phys. Vol. 21, 1161 (1982).

21. C.A. Brau, *Excimer Lasers*, ed. C.K. Rhodes (Berlin: Springer-Verlag, 1983).

22. S. Watanabe and A. Endoh, Appl. Phys. Lett., Vol 41, 1 (1982).

23. F. Flannery and T. Yang, Appl. Phys. Lett., Vol. 32, 327 (1978).

24. J. Coutts and C. Webb, Jour. Appl. Phys., Vol 59, 704 (1986).

25. J. Sheffield, *Plasma Scattering of Electromagnetic Radiation* (Academic, New York, 1975).

26. T.Y. Chang, Rev. Sci. Inst., Vol. 44, 405 (1973).

27. H. Houtman, A. Cheuck, A. Elezzabi, J. Ford, M. Laberge, W. Liese, J. Meyer, G. Stuart, and Y. Zhu, Rev. Sci. Inst., Vol. 64, 839 (1993)

28. J. Moore, C. Davis, M. Coplan, *Building Scientific Apparatus: a Practical Guide to Design and Construction* (Addison-Wesley, Redwood City, 1989).

29. A. DeSilva and G. Goldenbaum, *Methods of Experimental Physics*, Ch.3 Vol 19 (part A) (1970).

30. H. Hokanzono, K. Midorikawa, M. Obara, and T. Fujioka, J. Appl. Phys. Vol. 56, 680 (1984).